J Inorg Organomet Polym (2010) 20:183–212
DOI 10.1007/s10904-010-9358-5

REVIEW PAPER

Solid-State Nuclear Magnetic Resonance Spectroscopy: A Review of Modern Techniques and Applications for Inorganic Polymers

Alexey S. Borisov · Paul Hazendonk · Paul G. Hayes

Received: 28 January 2010 / Accepted: 29 March 2010 / Published online: 27 April 2010

Abstract The basic concepts of solid-state nuclear magnetic resonance (NMR) spectroscopy are explained in a clear and concise manner. First the reader is introduced to the principles of NMR spectroscopy and techniques that are most commonly utilized today. Next, an overview of advanced magic-angle spinning (MAS) NMR experiments, which can provide valuable insight into molecular structure, connectivity, dynamics, domains, and phases of inorganic polymers, is presented. The final chapter discusses the major classes of inorganic polymers, their properties and applications. It addresses their characterization including, if any, the role of solution and solid-state NMR spectroscopy, and provides prospective on potential applications of these techniques for the given class of material.

Keywords Solid-state nuclear magnetic resonance · MAS NMR · Spectroscopy · Inorganic polymers · Polysilanes · Polysiloxanes · Polysilazanes · Metal-containing polymers

1 Introduction

One of the primary foci of material science today is the development of novel polymeric materials and modification of existing ones, to ensure that they conform to health and safety concerns and meet the ever-increasing requirements imposed by modern technologies. In order to understand how to finely tailor the macroscopic properties of a polymer one must first understand how they relate to its structural features on an atomic scale. A variety of techniques for characterizing solid materials exist today, each employing different physical principles which impose limits on the types of properties and on the level of detail they can probe. X-ray diffraction, differential scanning calorimetry (DSC), thermogravimetric analysis (TGA), and gel permeation chromatography (GPC), are most commonly applied to studying polymers. In the case of semi-crystalline polymers X-ray diffraction is limited to providing unit cell dimensions of crystalline phases and cannot provide much insight into disordered phases. DSC gives only thermodynamic transition temperatures. Thus, most techniques do not provide structural and dynamic information at the atomic level. On the other hand, solid-state nuclear magnetic resonance (SSNMR) spectroscopy is not subject to these limitations and has proven to be an extremely robust and versatile tool for probing a broad range of parameters that are common to polymers.

As depicted in Fig. 1, there has been an abundance of solid-state NMR studies of polymers published between 1980 and 2009. The graph indicates that significant interest in solid-state NMR spectroscopy in the polymer community began to rise in 1990, where the number of annual publications on the topic in all journals increased 4-fold from 1990 to 1992. Since then, the amount of published work has been steadily increasing, almost reaching 800 manuscripts per year by 2009. This significantly increased interest is presumably due to the commercial availability of instruments, as well as the tremendous progress in pulse sequence development achieved in the past two decades.

Somewhat similar conclusions can be drawn for the Journal of Inorganic Chemistry and the Journal of Physical Chemistry, the Journal of Chemical Physics, Physical

A. S. Borisov · P. Hazendonk (✉) · P. G. Hayes
Department of Chemistry and Biochemistry, University of Lethbridge, 4401 University Dr, Lethbridge, AB T1K 3M4, Canada
e-mail: paul.hazendonk@uleth.ca

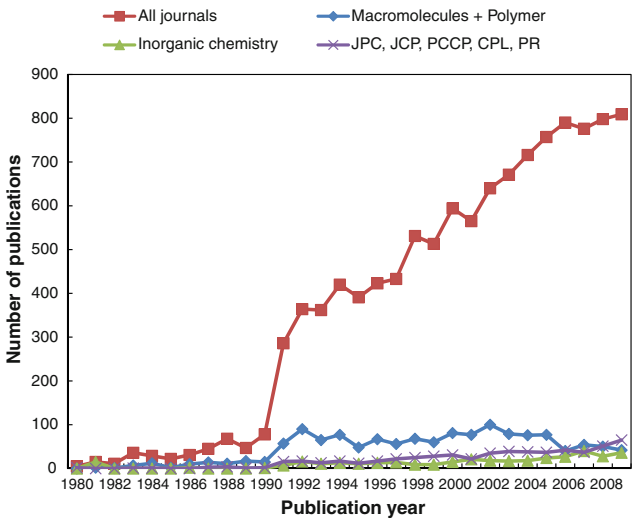

Fig. 1 Literature on solid-state NMR of polymers. *Lines* indicate the number of publications on the topic in the specified journal(s); Macromolecules and Polymer combined; Inorganic Chemistry; Journal of Physical Chemistry (JPC), Journal of Chemical Physics (JCP), Physical Chemistry Chemical Physics (PCCP), and Chemical Physics Letters (CPL) and Physical Review (PR) combined

Chemistry Chemical Physics, Chemical Physics Letters and Physical Review combined, where the number of publications increases approximately linearly over the period from 1992 to 2009.

In contrast, the trend seen in Macromolecules and Polymer indicates that after spiked interest in solid-state NMR spectroscopy in 1992, the number of papers published levels, and actually decreases slightly in the last 4 years. These specialized journals are generally considered the primary sources for publications of significant importance to polymer science. As the popularity of solid-state NMR spectroscopy as a versatile and comprehensive tool for studying polymers spread out across the scientific community, authors no longer needed to limit publications to macromolecules and polymer and began targeting a much wider array of journals. This notion is consistent with the behavior observed in the graph.

In the past decade there have been a number of excellent publications reviewing interesting examples of SSNMR applications for organic and biological polymer systems [1–6], most notably 'Multidimensional Solid-State NMR and Polymers' by Schmidt-Rohr and Spiess [7]. In contrast, relatively few solid-state NMR investigations of inorganic polymers have been published to date. It is possible that one of the main reasons for the lack of use of SSNMR in inorganic polymer science is due to the fact that historically spectrometer hardware and experimental methods were tailored for organic systems (^{1}H and ^{13}C nuclei). However, these instrumental limitations no longer remain and along with recent pulse sequence developments offer a myriad of techniques which can be readily applied to inorganic macromolecular solids. It is therefore the main goal of this contribution to introduce the inorganic polymer community to the basic concepts and theory of SSNMR, to demonstrate its versatility and power through selected examples of applications for inorganic polymers, and ultimately, to reveal the unrealized potential that SSNMR has to advance material science.

There have been a plethora of studies published in the past several years where magic-angle spinning (MAS) NMR spectroscopy was used as the primary technique for elucidating dynamics in various organic polymers [8–18]. Orientation-dependent dipolar couplings and chemical shift anisotropy (CSAs) often cause line broadening in NMR spectra of solids, and hence, need to be removed. However, under certain circumstances these interactions can be used to measure the rate and geometry of motion—such information is inaccessible via other spectroscopic methods. An excellent example of this is a study by Chen and Schmidt-Rohr, who observed the backbone dynamics in the perfluorinated ionomer, Nafion®, using measurements of the ^{19}F–^{13}C dipolar couplings along with ^{19}F and ^{13}C CSAs [12]. The reduced ^{19}F–^{13}C dipolar splitting and uniaxial CSAs suggested rapid uniaxial rotation of the backbone around the chain axis at ambient temperature with an amplitude of greater than 15°. Solid-state NMR spectroscopy illustrates the extent of the backbone "stiffness", which previously was not given significant consideration in molecular dynamics simulations of Nafion® [19].

Solid-state NMR spectroscopy has also been proven to be extremely useful in studying dynamics in polymer-based guest–host systems [17, 18]. For instance, a comprehensive review by Lu et al. presents SSNMR applied to a series of complexes formed with polymer guests included in small-molecule hosts, such as: urea, perhydrotriphenylene and cyclodextrins [17]. The combination of ^{13}C CPMAS solid-state NMR and molecular dynamics simulations provided conformational and dynamic information about polymer chains isolated from the bulk phase. Additional dynamic information about the guest and host were obtained via relaxation measurements, two-dimensional ^{13}C WISE (WIdeline-SEparation) experiments, cross-polarization dynamics and ^{2}H lineshape analyses. Relaxation measurements on ^{1}H in the rotating frame, $T_{1\rho}(^{1}H)$, detected through ^{13}C, were used to probe proton spin diffusion. This process is dependent on dipolar interactions, making it very sensitive to structural and dynamic aspects of the local environment, and thus was able to distinguish between the phase-separated and homogeneous structures of the complexes. These results allowed for the development of a model for single-chain dynamics independent from interchain processes in the bulk phase.

Another recent example of SSNMR spectroscopy applied to guest–host systems, this time involving polymers hosts, is a study by Albunia et al. [17]. Deuterium solid-state NMR was used to study dynamics of benzene-d_6 and 1,2-dichloroethane-d_4 (DCE) guests dissolved in the amorphous phase of polyethylene or in the cavities formed by nanoporous crystalline phases of syndiotactic polystyrene. In these systems slow molecular dynamics and a small degree of disorder in guest molecules ruled out the use of X-ray diffraction. Alternatively, deuterium solid-state NMR, not affected by disorder, can provide details on geometry and rates of restricted molecular motions taking place on the time scale of 10^5–10^8 Hz. The polymer hosts were used to reorient the guest molecules with respect to the magnetic field direction via uniaxial stretching of the film. Thus the geometry of the reorientational dynamics of the guests could be systematically studied through changes in the deuterium lineshape of the guest spectrum upon changing the stretching axis of the film.

SSNMR has made valuable contributions to the understanding of proton conductivity of polymer-electrolytes as is nicely illustrated in a few selected publications [12, 14, 20–27]. Ye et al. used ^{1}H MAS NMR to study proton mobility in the perfluorinated ionomer Nafion® and in sulfonated poly(ether ether ketone) (S-PEEK) [20]. They determined that the proton exchange between sulfonic acid groups and water, which occurs in both Nafion® and S-PEEK, is dependent on the water content as well as temperature. Measurements of activation energy for the proton transport led to the conclusion that under low humidity dried S-PEEK is a competitive proton conductor compared to Nafion®. Structure and dynamics conclusions were drawn on the basis of proton–proton dipolar coupling measurements via the Double-Quantum Filtering (DQF) method known as back-to-back (BABA). BABA can be tuned to measure weak dipolar couplings that would normally be undetectable due to rapid molecular motion or large distance ranges over which they occur. Discrimination on the basis of the strength of dipolar coupling interaction amounts to selection on the basis of proton mobility within the polymer and thus directly probes proton conductivity.

Solid-state NMR spectroscopy has been used extensively to study polymer morphology [9, 10, 13, 15, 16, 28–33]. An interesting example is illustrated by Yao et al. who studied the influence of morphology on chain dynamics in amorphous regions and chain diffusion between crystalline and amorphous domains within ultra-high molecular weight polyethylene [34]. Observed geometry of the conformational transitions obtained via measurements of ^{1}H–^{13}C dipolar couplings using Rotor-encoded Rotational-Echo DOuble-Resonance (ReREDOR) [35] and ^{13}C chemical shift anisotropy using Separation of Undistorted Powder patterns by Effortless Recoupling (SUPER) [36], were compared for samples crystallized from the melt and from solution. Chain diffusion observed via ^{13}C exchange spectroscopy exhibited profound differences in conformational transitions in the samples. Experimental data suggests that the chain diffusion between the crystalline and amorphous domains in the sample crystallized from solution is facilitated by axial motion of extended trans-conformers about the chain axis; it is significantly faster compared to the samples crystallized from the melt, where motions are significantly more isotropic.

Another interesting example demonstrating the utility of MAS NMR in the study of polymer morphology was recently reported by Zhang et al., whereby the dynamics and domain structure of poly(3-hydroxybutyrate) and poly(3-hydroxybutyrateco-3-hydroxyvalerate) were studied [15]. Using a combination of single-pulse excitation with magic-angle spinning (SPEMAS) and CPMAS ^{13}C experiments, the authors were able to observe separate signals from crystalline and amorphous domains of both the homopolymers and their co-polymers. Selection of crystalline and amorphous signals in ^{13}C spectra was achieved using the proton relaxation induced spectral editing (PRISE) experiment. These experiments showed that the crystallinity was 56–68% with a slight variation between samples. Spin-lattice relaxation in the rotating frame, $T_{1\rho}(^1H)$, measurements revealed that the two components differed significantly in mobility. These mobility differences make it possible to distinguish their signals and study them separately. Consequent proton spin-diffusion measurements were able to provide the domains sizes in the homopolymers and their co-polymers, which were estimated to be 15–76, 12–65 and 11–55 nm for the crystalline domains, and approximately 13, 24 and 36 nm for the amorphous domains.

In conclusion, solid-state NMR has made significant contributions to polymer science, as seen by the steady increase in the number of publications over the last decade. This spectroscopic method can no longer be considered just a supplementary technique; through constant improvements in instrumentation and pulse sequence design, solid-state NMR spectroscopy has became an independent, and often primary, tool for elucidating structural, dynamic and other information about polymers. On one hand, advanced experiments discussed within the context of this contribution provide a truly unique insight into properties of interest, which otherwise would be impossible to obtain. On the other hand, the concepts of solid-state NMR can be intimidating to the non-specialist; however, they are critical in order to understand pulse sequences and to appreciate their potential applications.

It is exactly for these reasons that this review will begin by introducing the basic principles of NMR spectroscopy,

which will provide the necessary background to understand the rudimentary solid-state NMR experiments. This approach attempts to rely on as little theory as practical and should be suited to anyone with a graduate chemistry background. The introduction is followed by an extensive overview of modern solid-state NMR techniques and their application to specific polymer problems. Select examples demonstrating the versatility and power of SSNMR are provided along with the discussion of prospective applications to inorganic polymer systems.

2 Nuclear Magnetic Resonance

2.1 Nuclear Spin and Magnetization

NMR is a spectroscopic technique that manipulates the interactions between magnetic moments of nuclei and magnetic fields. These interactions are strongly influenced by the local electronic environment of the observed nucleus providing unique insight into chemical and physical properties, and dynamics of materials in both liquid and solid states. Since its discovery independently by Felix Bloch and Edward Mills Purcell in 1946, NMR techniques have been rapidly developing from both instrumental and experimental design perspectives for both solids and liquids applications [37]. Today NMR has become an extremely powerful and versatile spectroscopic technique, whose application is growing rapidly in organic and inorganic chemistry, biological and materials science, as well as in medicine. It can no longer be considered a small subdiscipline in chemistry or physics, but is rapidly becoming a vast interdisciplinary field in its own right which is highly collaborative in practice.

Nucleons posses a number of intrinsic properties, such as charge, mass and angular momentum. This angular momentum is referred to as nuclear spin, and just like orbital angular momentum it is characterized by two quantum numbers: **I** and **M**. The nuclear spin quantum number **I** indicates the total angular momentum, and **M** represents the z-component of the angular momentum which can take $2\mathbf{I}+1$ values, from $-\mathbf{I}$ to $+\mathbf{I}$. This intrinsic angular momentum gives rise to magnetic moment $\vec{\mu}$:

$$\vec{\mu} = \gamma \hat{\boldsymbol{I}} \tag{1}$$

The proportionality constant, γ, is referred to as the magnetogyric ratio and is specific to each nucleus. The energy of interaction between an external magnetic field, $\vec{\mathcal{B}}_0$, and a nuclear magnetic moment depends on their respective orientation as given by:

$$E = -\vec{\mu} \cdot \vec{\mathcal{B}}_0 \tag{2}$$

By defining the magnetic field to be along the z-axis, the energy becomes dependent on the z-component of magnetization:

$$E = -\gamma \hat{I}_z B_0 \tag{3}$$

Energy sub-levels in the absence of external magnetic fields are degenerate, and the direction of the axis of the angular momentum is defined by isotropic distribution, as seen in Fig. 2.

In the presence of a magnetic field these states are no longer degenerate. The axis of angular momentum becomes aligned with the magnetic field, which is arbitrarily chosen to be along the z-axis. In the case of spin-1/2, according to $2\mathbf{I}+1$, two states are possible, $+1/2$ and $-1/2$, pointing upwards or downwards with respect to the external field, at an angle θ determined by initial orientation of the nuclear magnetic moment before the field was applied. This angle between spin polarization and an external magnetic field is constant with respect to time, as shown in Fig. 3, when ignoring the effect of external perturbations that lead to relaxation. The orientations parallel to the field have reduced magnetic energy, and therefore

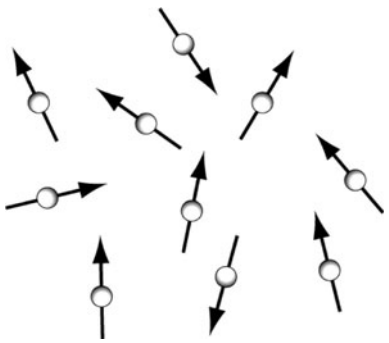

Fig. 2 Isotropic distribution of spin magnetic moments in the absence of an external magnetic field [38]

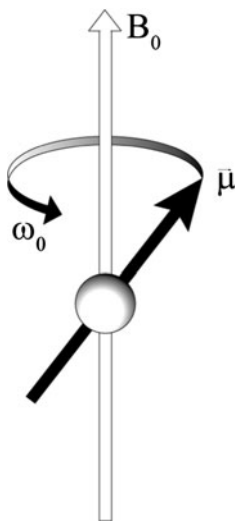

Fig. 3 Precession of the spin magnetic moment in the presence of an external magnetic field B_0 [38]

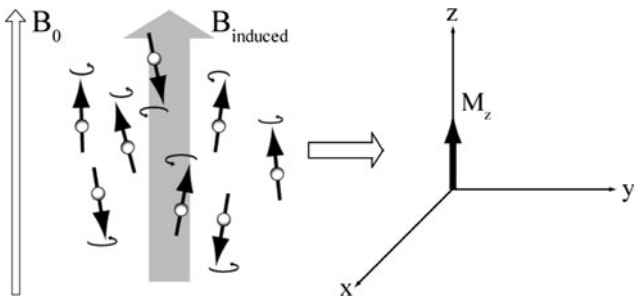

Fig. 4 Ensemble of spins precessing at ω_0 in the presence of an external magnetic field B_0 along the z-axis (*left*), and the corresponding longitudinal magnetization vector (*right*) [38]

are slightly more probable, according to the Boltzmann distribution.

The magnetic moment $\vec{\mu}$ experiences a torque perpendicular to its direction causing it to rotate about an axis defined by the magnetic field direction. The frequency of this motion is specific to each type of nucleus and is referred to as the nuclear Larmor frequency ω_0:

$$\omega_0 = -\gamma B_0 \tag{4}$$

On the macroscopic level, a sample in the presence of a magnetic field consists of an ensemble of randomly oriented spin magnetic moments, each precessing around the direction of the magnetic field at its Larmor frequency, randomly distributed in phase. Recall that there is a slight preference for the magnetic moments being aligned parallel with the field. This gives rise to a net longitudinal magnetization, which is cylindrically symmetrical at any time along the magnetic field and therefore has no transverse component (shown in Fig. 4).

The induced longitudinal polarization is best detected when perpendicular to the field. If it were possible for all of the spins to precess in phase with each other, a net transverse magnetization rotating at the Larmor frequency would result. This phase coherence can be achieved by applying a strong radio-frequency pulse on resonance with the Larmor frequency. The net effect of this pulse is to rotate the bulk longitudinal polarization into the transverse plane, as shown in Fig. 5.

2.2 Relaxation

Spins experience constant perturbations from small locally random time-dependent magnetic fields due to neighboring spins and other electronic interactions. Through this 'diffusion-like' process the spins randomly re-orient, and hence, have an isotropic orientational distribution in the absence of an external magnetic field. When a strong external magnetic field is applied along the z-axis, it causes the spins to randomly 'walk' towards the z-direction, generating a net bias in the spin orientations over time. The rate of reorientation of the spins, and the corresponding build-up of macroscopic longitudinal magnetization is characterized by a longitudinal relaxation time constant, T_1. Longitudinal relaxation largely depends on the time-scale of fluctuating local fields caused by nearby molecular motion, which in turn is a function of temperature and viscosity of the material; therefore, T_1's can be in the range of millisecond to days or weeks. When the external field is turned off, the net polarization is lost over time due to the same perturbations. Time-dependence of the longitudinal magnetization can be characterized by the curve depicted in Fig. 6.

Recall that a radio-frequency pulse creates phase coherence between spins. Fluctuations caused by the local

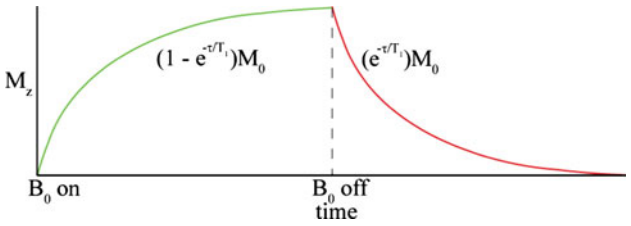

Fig. 6 When magnetic field B_0 is turned on, longitudinal magnetization builds-up exponentially at a rate defined by T_1. After B_0 is turned off, longitudinal magnetization starts decaying at a same rate [38]

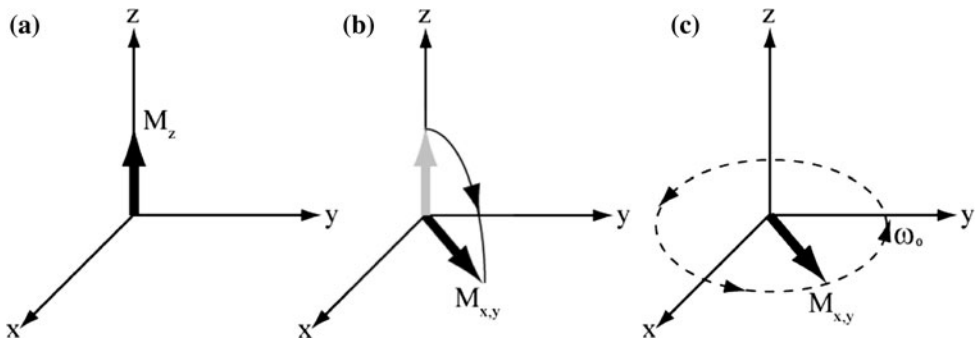

Fig. 5 **a** The z-component of the net magnetization; **b** the magnetization rotated to the transverse plane by application of a $\pi/2$ RF pulse; **c** Larmor precession of the transverse polarization [38]

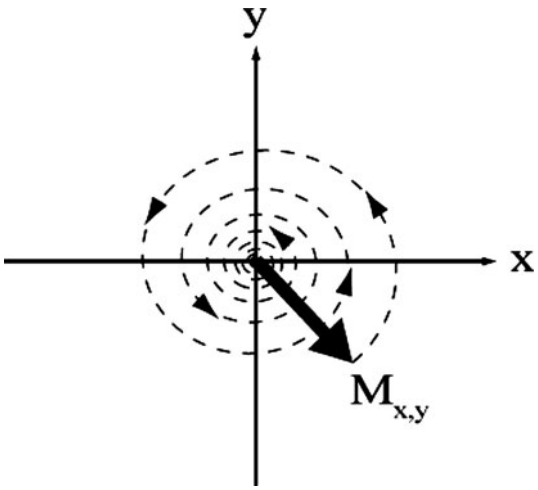

Fig. 7 Vertical projection of decaying transverse magnetization

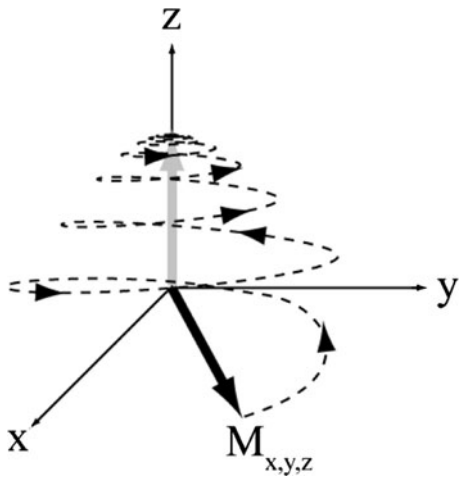

Fig. 9 Relaxation of the transverse magnetization

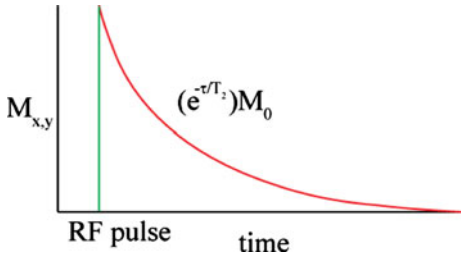

Fig. 8 Decay of transverse relaxation at a rate defined by T_2

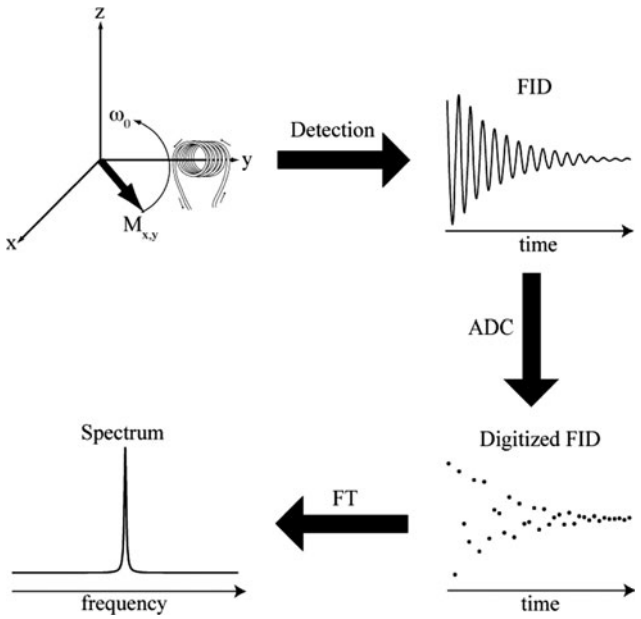

Fig. 10 Design of an NMR experiment

time-dependent magnetic fields result in the loss of this synchronization over time. This loss of coherence can be observed as a decaying transverse magnetization; hence, it can be thought of as moving on a spiral-like trajectory in the transverse plane, as illustrated in Fig. 7.

The rate of this decay is characterized by the transverse relaxation time constant, T_2, which is different from T_1. Most commonly $T_1 \geq T_2$ in liquids, and $T_1 \gg T_2$ in solids. The exponential relaxation curve is shown in Fig. 8.

When considering transverse and longitudinal components simultaneously, the magnetization can be thought of as a rotating vector 'walking' from the transverse plane to the direction of the applied magnetic field along a conical path, as seen in Fig. 9.

2.3 NMR Experiment

The magnitude of the transverse magnetization is small; however, it is detectable. The rotating magnetic moment in the transverse plane gives rise to an oscillating magnetic field, which in turn induces an electric current in a coil, if its winding axis is along the *xy*-plane. This weak electric signal oscillates and decays over time just like the transverse magnetization, and is called a Free Induction Decay (FID). The FID is amplified, digitized (ADC) and subsequently transformed to the frequency domain via a Fourier transformation (FT). The resulting NMR spectrum, which is a plot of signal intensity as a function of frequency, has a peak centered at the Larmor frequency with full width at half height (FWHH) determined by $1/T_2$ (Fig. 10).

NMR experiments are conventionally described with a pulse sequence timing diagram, which shows all experimental events in the order of their appearance in time. The very basic pulse sequence contains an excitation radiofrequency pulse, where its length is given by the angle by which it rotates longitudinal magnetization, followed by detection of the FID, as seen in Fig. 11. More advanced

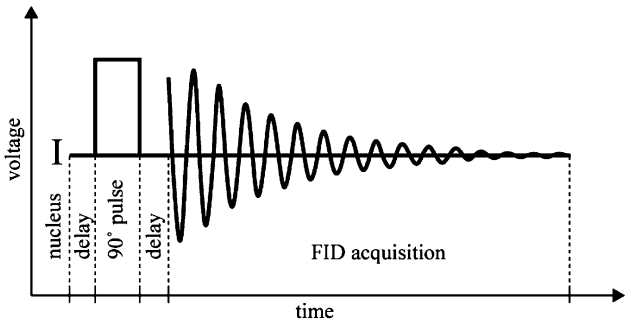

Fig. 11 Pulse sequence diagram of a basic NMR experiment on nucleus **I**

experiments include decoupling and polarization transfer, and may involve multiple nuclei simultaneously.

2.4 Coherences

An ensemble of spins can be thought of being composed of a mixture of states. For instance, an external magnetic field causes the spin magnetic moments to precess about the field's direction without synchronization of their phases. In other words, there is no phase coherence between the spins. The probability of 'up'-wise and 'down'-wise orientations with respect to the magnetic field is nearly equal (Fig. 12a); hence, at equilibrium only a very small excess of spins are oriented along the z-axis giving rise to a net longitudinal polarization (Fig. 12b). With the application of a resonant 90° radio frequency pulse it is possible to equalize spin populations and impose phase synchronization (coherence) between the spins, giving rise to two counter-rotating components of transverse magnetization. Each of these transverse magnetizations are in turn a combination of x- and y-magnetizations in their corresponding rotating frames at $\pm\omega_0$. These phase coherent time-dependent transverse magnetizations are referred to as positive and negative single-quantum coherences (SQCs). By convention, NMR experiments are tuned to detect negative single-quantum coherences; however, positive single-quantum coherences can be measured as well.

In principle, an ensemble of single-spin systems can be thought of as being composed of a combination of the four states shown above, which in turn is related to the vector components of the spin magnetization. Quantum mechanics makes use of spin operators to describe the state of a spin system; therefore, in the case of a single spin, **I**, we must consider four operators: **1**, $\mathbf{I}_z$, $\mathbf{I}_+$ and $\mathbf{I}_-$. Operator **1**, also known as the identity operator, represents an ensemble with no net polarization; $\mathbf{I}_z$ indicates the net longitudinal polarization along the magnetic field direction, which by convention corresponds to the z-component, representing the net z-magnetization $\mathbf{M}_z$; $\mathbf{I}_+$ and $\mathbf{I}_-$ represent phase coherence between the spins that oscillate at $\pm\omega_0$ and are

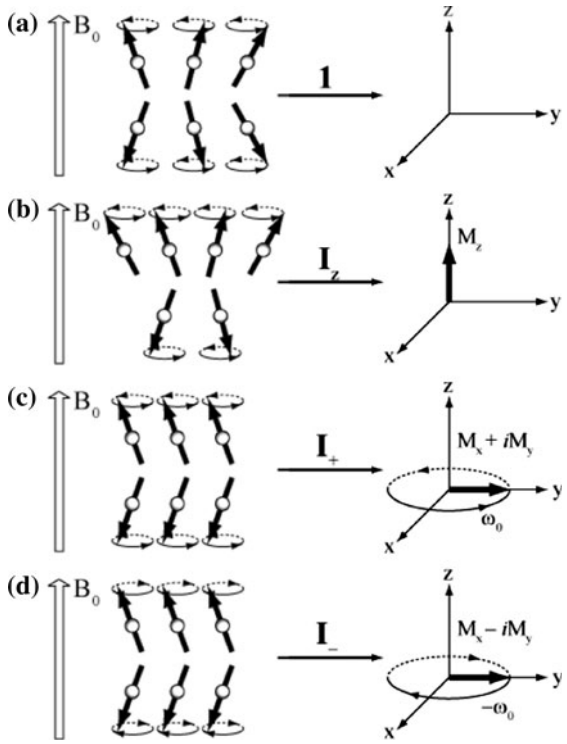

Fig. 12 Physical interpretation of the states of an ensemble of single-spin systems: **a** non-polarized state; **b** net longitudinal polarization; **c** positive single-quantum coherence; **d** negative single-quantum coherence

related to the transverse magnetization in the rotating frame as $\mathbf{M}_x + i\mathbf{M}_y$, and $\mathbf{M}_x - i\mathbf{M}_y$, respectively.

For a coupled spin pair (**IS**) one has to represent the ensembles of the two spins simultaneously, and the simple one-spin correspondence between the operators and the magnetization vectors no longer applies. Instead, one must describe the system using products of the two spin operators representing the states of the individual ensembles. For every state of **I** four states of **S** must be considered; thus, a set of 16 operators is required to fully describe the coupled spin system.

At equilibrium, there are no coherences between spins. Hence, the system is given by a combination of the states: **11**, $\mathbf{I}_z\mathbf{1}$, $\mathbf{1S}_z$ and $\mathbf{I}_z\mathbf{S}_z$. The state **11** represents non-polarized contribution to the ensemble, and is thus ignored (Fig. 13a). The net longitudinal polarization of one spin is correlated to the state of the other spin; therefore, the z-magnetization of **I** and **S**, $\mathbf{I}_z\mathbf{1}$ and $\mathbf{1S}_z$ are each represented by two parallel (in-phase) polarization vectors along the z-axis (Fig. 13b). When both spins are polarized along the z-axis simultaneously, as in $\mathbf{I}_z\mathbf{S}_z$, the two magnetization vectors are antiparallel (anti-phase) pointing in opposite directions (Fig. 13c).

When a resonant 90° pulse is applied on a two-spin system, the net polarization of one spin, for example ($\mathbf{I}_z\mathbf{1}$),

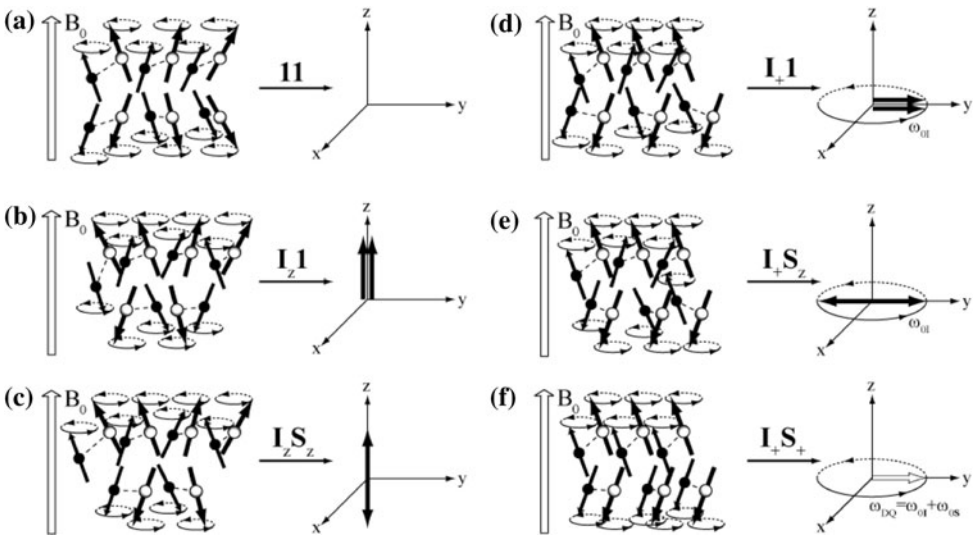

Fig. 13 Physical representation of the states of an ensemble of **IS** spin systems: **a** both spins are non-polarized; **b** spin **I** is polarized along the *z*-axis while spin **S** is in the non-polarized state (**1S**$_z$ state is not shown); **c** both spins are polarized along the *z*-axis; **d** in-phase positive single-quantum coherence of spin **I** (**I**$_-$**1**, **1S**$_+$ and **1S**$_-$ states are not shown); **e** anti-phase positive single-quantum coherence of spin **I** (**I**$_-$**S**$_z$, **I**$_z$**S**$_+$ and **I**$_z$**S**$_-$ states are not shown); **f** positive double-quantum coherence (**I**$_-$**S**$_-$, **I**$_+$**S**$_-$ and **I**$_-$**S**$_+$ states are not shown)

is converted into single-quantum coherence, $\mathbf{I}_+\mathbf{1}$, while the other spin remains in the non-polarized state. This can be represented by two parallel vectors rotating in-phase in the transverse plane at $+\omega_0$ (Fig. 13d). Therefore, after a pulse is applied to a spin system at equilibrium there are four possible states: $\mathbf{I}_+\mathbf{1}$, $\mathbf{I}_-\mathbf{1}$, $\mathbf{1S}_+$ and $\mathbf{1S}_-$. These are referred to as in-phase single-quantum coherences. The two positive SQC's for each spin, correspond to the two components of the in-phase doublets in the spectrum.

During a delay period, usually after a pulse, the system typically evolves under chemical shielding and scalar coupling interactions. Under the influence of the former an in-phase SQC state remains unchanged oscillating according the frequency of the spin with net transverse polarization. For example, as shown in Fig. 13d, $\mathbf{I}_+\mathbf{1}$ evolves according to $\omega_{0\mathrm{I}}$. By contrast, under the influence of the latter, the non-polarized spin of the in-phase SQC oscillates between the non-polarized and polarized state at the frequency of the coupling interaction. For instance, the in-phase $\mathbf{I}_+\mathbf{1}$ state interchanges between itself and the anti-phase state, $\mathbf{I}_+\mathbf{S}_z$ at the frequency of the coupling interaction. As a result the initial four SQCs that exist after a 90° pulse is applied to the equilibrium state of the spin pair give rise to four additional anti-phase SQC's: $\mathbf{I}_+\mathbf{S}_z$, $\mathbf{I}_-\mathbf{S}_z$, $\mathbf{I}_z\mathbf{S}_+$ and $\mathbf{I}_z\mathbf{S}_-$. These new types of SQCs can be represented by two vectors rotating in the transverse plane with opposite phase (Fig. 13e), thus the name anti-phase single-quantum coherences. On one hand, anti-phase coherences are highly desirable as they play an important role in coherence transfer between nuclei. On the other hand, they give rise to undesirable anti-phase doublet signals in the spectrum and need to be removed prior to detection.

Using anti-phase SQC's it is possible to create zero- and double-quantum coherences, via the application of additional RF pulses. Positive and negative double-quantum coherences (DQCs), $\mathbf{I}_+\mathbf{S}_+$ and $\mathbf{I}_-\mathbf{S}_-$, can be represented by two parallel vectors rotating either clockwise or counter-clockwise in the transverse plane, at $\omega_{\mathrm{DQ}} = \pm\,\omega_{0\mathbf{I}} \pm \omega_{0\mathbf{S}}$ (Fig. 13f). Correspondingly, two counter-rotating vectors give rise to zero-quantum coherences, $\mathbf{I}_+\mathbf{S}_-$ and $\mathbf{I}_-\mathbf{S}_+$. Coherences of this order, generally known as multiple-quantum coherences, cannot be readily observed and need to be converted into in-phase SQC prior to detection. DQC's are important in the coherence transfer and make it possible to select signals from a desired origin while filtering out unwanted signals. Some of the experiments that incorporate evolution of double-quantum coherences will be explored in greater detail in the next chapter.

The concept of coherences is crucial for the understanding of the operation of NMR experiments. The effect of an NMR experiment upon the spin system can be neatly described by following the coherences encountered at various stages during the experiment. A coherence transfer diagram presents the changes in coherences on the nuclei as a function of the pulses and periods of evolution during the experiment. In order to illustrate this, let us consider a simple one-pulse experiment. As we have discussed previously, at equilibrium there is no coherence between spins and an NMR signal cannot be detected. A subsequent 90° pulse creates coherences of order ± 1 (positive and negative SQC), as shown in Fig. 14a. Since we are interested in detecting only one coherence, the unwanted coherence needs to be removed. This is achieved by using certain pulse phase cycles which eliminate the undesired coherence and leave only the single-quantum coherence of interest (by convention chosen as -1) that gives rise to an NMR signal.

Most NMR experiments consist of multiple RF pulses leading to a large number of coherence pathways that can be undertaken. For example, Fig. 14, b shows a coherence

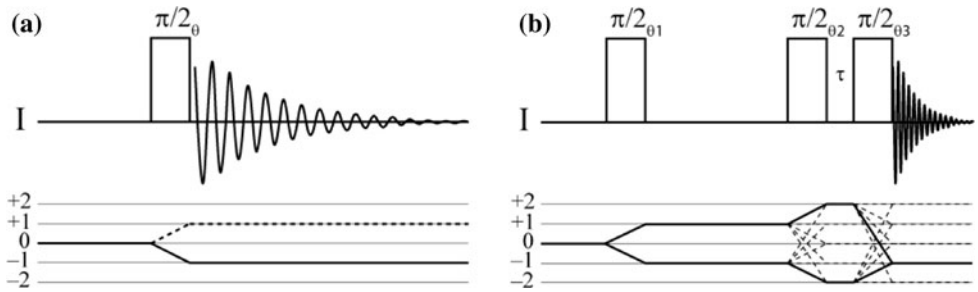

Fig. 14 Coherence pathway diagram for an arbitrary one-pulse experiment (**a**) and DQF COSY experiment (**b**)

pathway for a Double-Quantum Filtered COrrelation SpectroscopY (DQF COSY) experiment. In this case, an initial 90° pulse creates ±1 coherences, which are converted to coherences of various orders with a second pulse. Unwanted coherences are filtered out using proper phase cycles, and the desired coherences are converted into negative single-quantum coherence with a third 90° pulse at the end of the experiment.

In summary, NMR experiments are often discussed within the context of coherence pathways and typically start at equilibrium and end with in-phase single-quantum coherences that give rise to a detectable signal. With carefully designed pulse sequences it is possible to manipulate and transfer coherences between nuclei throughout an experiment to achieve a specific outcome, such as correlation of various spin sites, or selection of signals based on spin–spin interactions.

2.5 Chemical Shielding

In principle, an isolated spin-1/2 should give rise to a single peak which is characterized by a Lorentzian distribution and appears at its Larmor frequency. In NMR experiments, however, this is not generally the case. A phenomenon known as shielding causes a slight shift of the resonance frequency of the signals with respect to the Larmor frequency, where this offset can be approximated by the frequency of a reference compound particular to each nucleus of interest. This is called the chemical shift and is expressed in parts per million (ppm) of the reference frequency, so that it is independent of the field strength used:

$$\delta_i = \frac{\nu_i - \nu_{ref}}{\nu_{ref}} \tag{5}$$

Shielding arises due to local magnetic fields, $B_{induced}$, caused by currents in the electron density surrounding the nucleus. As a result the net magnetic field experienced by the nucleus is altered, as shown in Fig. 15.

This shielding interaction depends on the orientation of the molecular frame in which the currents are generated, with respect to the external field, where the vector of the induced magnetization is related to the vector of the

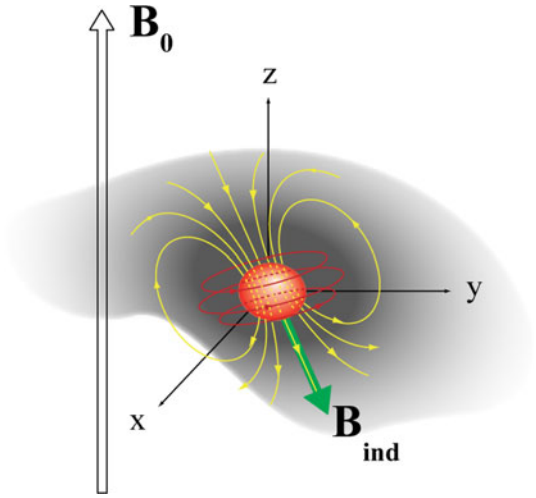

Fig. 15 A magnetic field, B_{induced}, generated by currents in the electron cloud surrounding the nucleus in the presence of an external magnetic field, B_0

applied magnetic field through the chemical shift tensor, $\hat{\hat{\delta}}$, as follows:

$$\vec{\mathcal{B}}_{induced} = \hat{\hat{\delta}} \cdot \vec{\mathcal{B}}_0 \tag{6}$$

The chemical shift tensor is described by a 3 × 3 matrix of the following form:

$$\hat{\hat{\delta}} = \begin{vmatrix} \delta_{xx} & \delta_{xy} & \delta_{xz} \\ \delta_{yx} & \delta_{yy} & \delta_{yz} \\ \delta_{zx} & \delta_{zy} & \delta_{zz} \end{vmatrix} \tag{7}$$

The tensor is represented in the laboratory frame, and is often transformed to its own reference frame, referred to as its Principal Axis System (PAS), as shown in Fig. 16.

The principal components of the CS tensor, δ_{jj}, are the eigenvalues of $\hat{\hat{\delta}}$. Its eigenvectors, $\vec{u}_{jj}$, are the unit vectors defining the axes of the PAS frame. The corresponding Eigen-representation of the tensor matrix is shown below:

$$\delta_{PAS} = \begin{vmatrix} \delta_{11} & 0 & 0 \\ 0 & \delta_{22} & 0 \\ 0 & 0 & \delta_{33} \end{vmatrix} \tag{8}$$

$$u = |\vec{u}_1|\vec{u}_2|\vec{u}_3| \tag{9}$$

$$\hat{\hat{\delta}} = \mu^{-1} \cdot \delta_{PAS} \cdot \mu \tag{10}$$

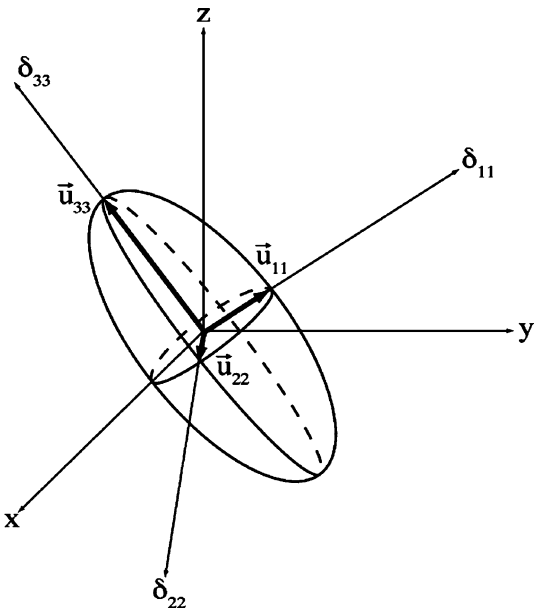

Fig. 16 Principle axis system of the chemical shift tensor

The average of the tensor is known as a relative isotropic chemical shift, δ_{iso}, and is defined as follows:

$$\delta_{iso} = \frac{1}{3}(\delta_{11} + \delta_{22} + \delta_{33}) \tag{11}$$

Correspondingly, the absolute isotropic chemical shift, σ_{iso}, has a similar form:

$$\delta_{iso} = \frac{1}{3}(\sigma_{11} + \sigma_{22} + \sigma_{33}) \tag{12}$$

By convention, the principal components are assigned as follows: [38]

$$|\delta_{33} - \delta_{iso}| \geq |\delta_{11} - \delta_{iso}| \geq |\delta_{22} - \delta_{iso}| \tag{13}$$

Recall that the anisotropic nature of the shielding interaction causes a distribution in Larmor frequencies of the nuclei when there is a corresponding distribution in orientations, as in a powder sample. The range over which the distribution of frequencies occurs is related to the chemical shift anisotropy (CSA), $\Delta\delta$, which has the following form:

$$\Delta\delta = \delta_{33} - \delta_{iso} \tag{14}$$

The shape of the distribution is characterized by the chemical shift asymmetry parameter, η_{CS} [38]:

$$\eta_{CS} = \frac{\delta_{22} - \delta_{11}}{\Delta\delta} \tag{15}$$

The CSA interaction affects the spectra of liquids and solids very differently. In liquids, rapid molecular motion averages out the anisotropy of the spin orientations leaving one narrow peak at the isotropic chemical shift, δ_{iso}. This rapid motion causes the CSA term to give rise to randomly

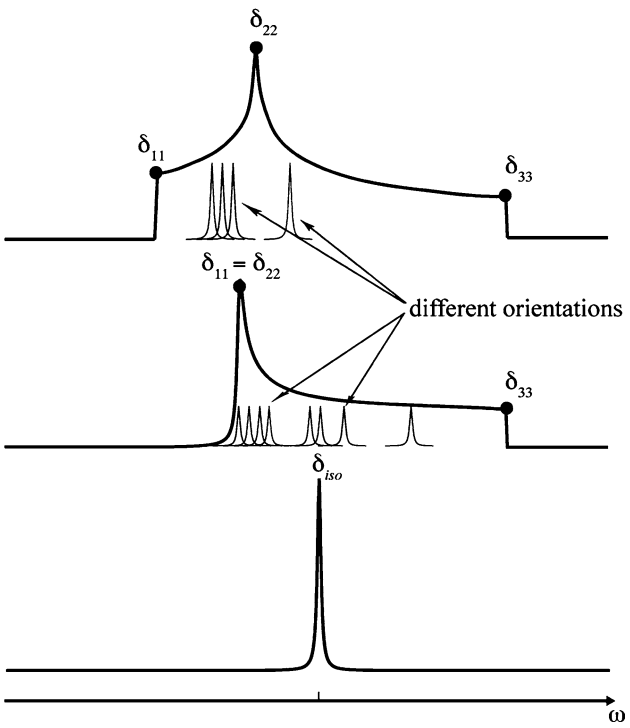

Fig. 17 Inhomogeneous line broadening mechanisms in NMR spectra caused by CSA. A powder pattern characterized by three different tensor components (*top*); a powder pattern characterized by a reduced chemical shift tensor in the case of axial symmetry along the bond axis (*middle*); a single peak at δ_{iso} as a result of fast isotropic motion (*bottom*)

fluctuating fields, and thus, provides a very efficient relaxation mechanism. As a result molecules with large CSAs can have very different relaxation times from those with much smaller CSAs, depending on experimental conditions such as temperature and viscosity. Solid-state experiments are normally performed on powders which consist of a large number of crystals, each having different orientation with respect to the applied magnetic field. Consequently, the CSA causes inhomogeneous broadening of the signal. The broad shape of the signal is the result of superimposition of peaks with different chemical shifts due to the various crystal orientations, and is referred to as a powder pattern (shown in the top of Fig. 17).

Tensor components can be scaled down in molecules that exhibit fast dynamics. For example, a methyl group that has rapid rotation about the CH_3–X bond axis leads to axial symmetry in the tensor along the bond which results in two of its principal components becoming equal (Fig. 17, middle). Finally, fast isotropic motion causes all three tensor components to become equalized; hence, all orientations have the same shielding, leaving one narrow peak at δ_{iso}, as seen in the bottom of Fig. 17. In short, the symmetry reflected by the tensor components is the result of a combination of the symmetry in the electron density

surrounding the nucleus and the symmetry of any motion that the system undergoes.

2.6 Nuclear Spin Interactions

The magnetic moment of a nuclear spin often interacts with the magnetic field of another spin. This interaction is called spin-spin coupling and occurs between same type (homonuclear) or different types (heteronuclear) of nuclei. Two modes of coupling are possible. The first is a direct interaction between the spins while the other is mediated through the electrons and is referred to as indirect coupling (*J*-coupling). The second mode involves polarizing electrons surrounding one nucleus, which gives rise to a magnetic field at the site of the second nucleus. This indirect dipole-dipole interaction causes spins to be sensitive to their neighboring spins giving rise to multiplet peak structures observed in the spectra of most liquids. This is most routinely exploited in the determination of molecular structures, via solution-state NMR spectroscopy. The *J*-coupling is also observed in the solid state, where it is orientationally dependent. Only its isotropic value is observed in solution.

Couplings can also be experienced directly between the magnetic dipole moments of nuclei through space, which is known as direct dipolar coupling, *D*. This interaction is characterized by the angle between the internuclear vector and the external magnetic field (as seen in Fig. 18), and by the coupling constant, b_{IS} [39]:

$$D_{IS} = b_{IS}\frac{1}{2}\left(3\cos^2\theta - 1\right) \tag{16}$$

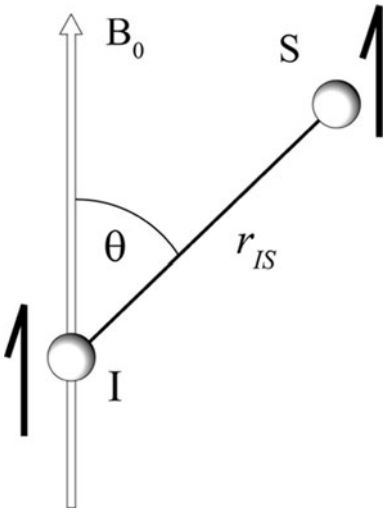

Fig. 18 The direct dipolar coupling between two spins, **I** and **S**, in the presence of an external magnetic field, B_0

The coupling constant between spins **I** and **S** is proportional to their magnetogyric ratios and to the internuclear distance, *r*:

$$b_{IS} = \frac{\hbar\mu_0\gamma_I\gamma_S}{4\pi r_{IS}^3} \tag{17}$$

The direct dipolar coupling is characterized by a traceless tensor, which means that it has an isotropic value of zero. This implies that the direct dipolar coupling is lost in liquids due to fast molecular motion. Solids, however, can exhibit very strong dipolar coupling, ranging from a few hertz to 100s of kHz.

Strong homonuclear couplings give rise to homogenous line broadening which can severely limit spectral resolution. Such interactions are especially strong and frequent in the case of abundant nuclei with large magnetogyric ratios, such as ^{1}H, where linewidths of 10s to 100s of kHz are common and spectra lack sufficient resolution to give detailed structural information. Consequently, ^{1}H is not commonly used directly. In contrast, ^{13}C is only 1% abundant and has a small magnetogyric ratio which results in weak rarely occurring homonuclear interactions. Hence, no homogeneous line broadening occurs and high resolution is possible even at modest spinning rates. Heteronuclear interactions from ^{1}H do not give rise to homogeneous line broadening and can be efficiently suppressed using decoupling sequences which will be explored further. Thus, ^{13}C{^{1}H} (^{1}H decoupled) MAS spectroscopy is routine. Ultimately, it is crucial to have experimental control over coupling so that it can be either suppressed to improve spectral resolution, or introduced to measure internuclear distances and determine connectivity.

Nuclear spin interactions become further complicated in the case of quadrupolar nuclei (spin > 1/2). In such a situation the electric charge distribution is no longer spherically symmetrical and interacts with surrounding electric field gradients depending on the geometry and orientation of the nuclei within the molecule. In solution, this often leads to very rapid relaxation of the quadrupolar nucleus and any other nucleus strongly coupled to it causing such nuclei to be very difficult to observe. Quadrupolar interaction is beyond the scope of this work and is the subject of an entire sub-discipline of NMR spectroscopy where unique specialized techniques have been developed to obtain high resolution from systems that would otherwise have linewidths ranging anywhere from tens of kHz to several MHz wide. Several excellent reviews are available on this topic [40–42].

2.7 Magic-Angle Spinning

Since dipolar coupling interactions are dependent on the direction of the coupling vector with respect to the external

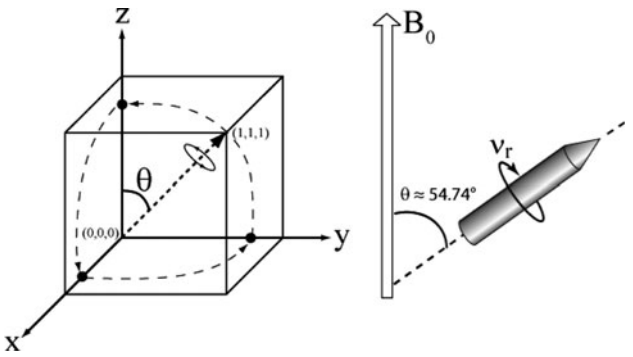

Fig. 19 Geometrical interpretation of the magic angle (*left*); sample rotation at the magic angle in solid-state NMR (*right*)

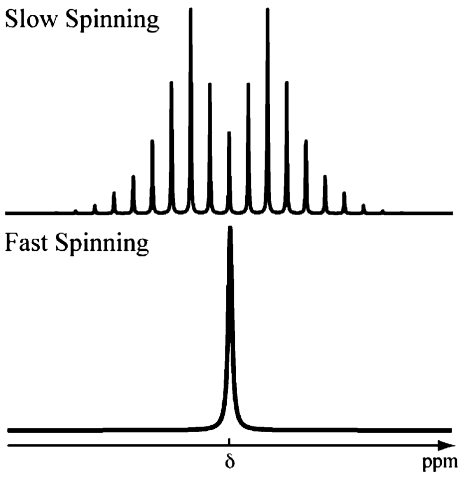

Fig. 20 MAS NMR spectrum with a sideband pattern due to insufficient spinning speed (*top*); the same spectrum but obtained at higher spinning speed (*bottom*)

magnetic field, they can be eliminated if the internuclear vector between two spins is inclined with respect to the applied field by the magic angle, given by:

$$\theta = \arccos\frac{1}{\sqrt{3}} \approx 54.74^\circ \qquad (18)$$

The magic angle can be defined as the angle between the z-axis and the body diagonal of a unit cube. Rotating an object about the direction of this diagonal would equally interchange its respective x, y, z coordinates and give rise to the equivalent to isotropic motion, as seen in the left hand side of Fig. 19. MAS NMR experiments on solids attempt to average out the orientational dependence of the nuclear spin interactions and reduce the inhomogeneous and homogeneous broadening, significantly improving the spectral resolution [43–46] (shown in Fig. 19, right).

Strong homonuclear couplings that give rise to homogeneous line broadening can only be effectively suppressed using spinning speeds exceeding the magnitude of the coupling interactions. This is not often achievable at even

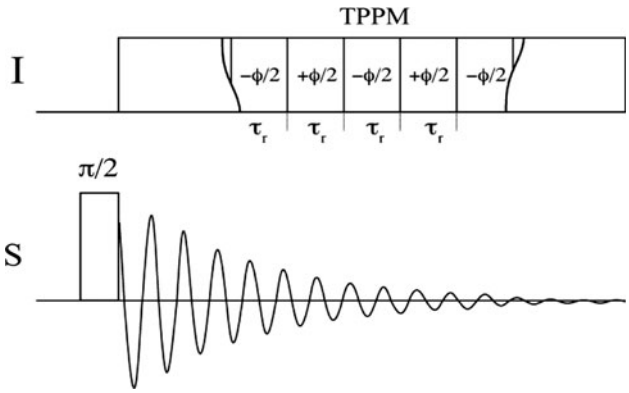

Fig. 21 Pulse sequence diagram of an MAS NMR experiment with TPPM heteronuclear decoupling of spin **I**

modern limits of spinning speed for ^{1}H and in some materials for ^{19}F and ^{31}P as well, where high resolution can remain elusive. Alternatively, heteronuclear coupling leads to inhomogeneous line broadening which is effectively removed under MAS conditions. If the interactions are too strong to be removed by MAS, the spectrum will exhibit a pattern of side-bands, where the isotropic line is surrounded by lines on both sides separated in frequency by the spinning speed, as seen in Fig. 20.

2.8 Decoupling Sequences

Strong dipolar spin interactions often result in splitting and inhomogeneous line broadening in NMR spectra, and hence need to be removed as they limit spectral resolution. Under the correct circumstances, they can be controlled, where the couplings provide useful information about the spin's electronic surroundings and internuclear distances, and hence can be highly desirable.

Decoupling sequences form a class of NMR techniques employed in both liquids and solids to remove heteronuclear spin coupling interactions. A variety of such methods is routinely implemented today and is always under development.

One such sequence of note is the Two Pulse Phase Modulation (TPPM) developed by Griffin and co-workers [47]. It consists of a train of rotor-synchronized RF pulses with alternating phases ($-\phi/2$, $+\phi/2$, $-\phi/2$…), as illustrated in Fig. 21. TPPM decoupling has been shown to be significantly more efficient in removing heteronuclear couplings under MAS conditions compared to conventional continuous-wave (CW) irradiation, where performance is offset dependent, and thus, ineffective for systems with large CSAs. The rotor-synchronized $\pm\phi/2$ phase modulation reduces offset-dependence of the decoupling sequence, increasing its performance, in particular for nuclei with broad frequency ranges, such as ^{19}F [47].

As mentioned earlier, high resolution in ^{1}H MAS NMR spectroscopy is often elusive due to strong homonuclear dipolar interactions. In such cases, fast magic-angle spinning is combined with radio-frequency irradiation, known as Combined Rotation and Multiple Pulse Spectroscopy (CRAMPS) [48]. Several recently developed CRAMPS sequences include the Decoupling Using Mind Boggling Optimization (DUMBO) [49–51], Frequency Switched Lee-Goldburg (FSLG) [52], Phase-Modulated Lee-Goldburg (PMLG) [50, 53–56] and Smooth Amplitude-Modulated (SAM) [53] methods. These homonuclear decoupling techniques have proven very effective in enhancing resolution in NMR spectra under fast MAS conditions, as well as in suppressing spin diffusion which results from strong homonuclear dipolar interactions (as discussed in Sect. 2.11) [57].

The FSLG decoupling sequence makes use of recent advances in RF timescale control. It consists of a train of RF pulses with rapidly switching frequencies and phases that are shifted by π every rotation period. FSLG offers certain advantages over other decoupling schemes, such as short duty cycle, tolerance to RF errors and phase shifts, and simple calibration of parameters [58].

In some cases even further improvements of the heteronuclear decoupling efficiency can be achieved using a Carr-Purcell-type sequence with an XY-16 phase cycle, consisting of a train of 16 rotor-synchronized high-power π pulses.

The XY-16 decoupling sequence compensates for pulse imperfections, reduces offset dependence, and avoids short duty cycles. It allows for the long acquisition times required for high resolution, as the high power π pulses are applied every rotor period, instead of using continuous high power irradiation. This avoids RF breakthrough from the decoupling channel to the detection channel, which imposes limits on the powers and duration over which decoupling can be employed. This decoupling sequence is particularly very effective,[59] as the rotor-synchronized 180° pulses with the XY phase cycle refocus the heteronuclear coupling interactions over a large frequency range at the end of each rotation period, and thus is especially useful when decoupling nuclei with large CSAs, such as ^{19}F. When performing simultaneous decoupling with continuous irradiation methods, such as CW and TPPM, the power limits are particularly prohibitive, and hence it is difficult to implement on two strong abundant nuclei at the same time. In contrast, XY-16 decoupling does not suffer from these power limitations and can be readily applied to several nuclei at once (e.g. ^{13}C{^{1}H,^{19}F}). Simultaneous high power decoupling in ^{13}C MAS NMR spectroscopy has been applied in the study of fluoropolymers [59] and polyphosphazene [32] (shown in Fig. 22) using XY-16 decoupling, where dramatic improvements in ^{13}C spectral resolution were achieved.

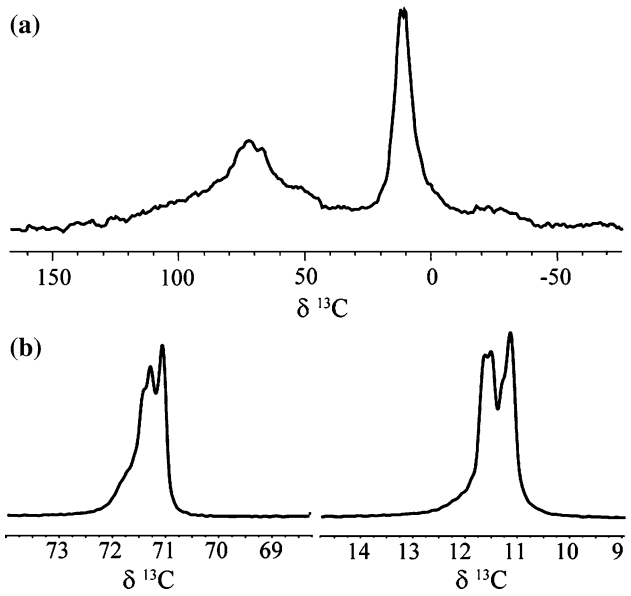

Fig. 22 **a** ^{13}C{^{1}H, ^{19}F} MAS NMR spectrum of poly[*bis*(trifluoroethoxy)phosphazene] (PBFP) using standard CW decoupling. Signals at 71 and 11 ppm are assigned to CF_3 and CH_2 carbons, respectively. The linewidths are on the order of 25–35 ppm obscuring any definite observation on polymer morphology; **b** same as (**a**), but using simultaneous high power XY-16 decoupling. Expansions show dramatic improvement in resolution of both the CF_3 and the CH_2 signals

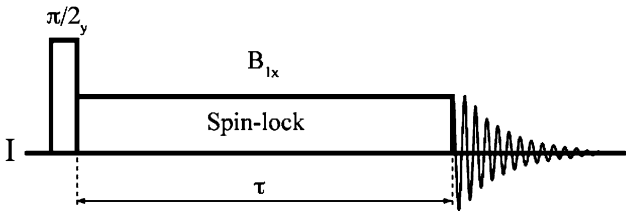

Fig. 23 A basic spin-lock pulse sequence for measuring $T_{1\rho}$

2.9 Spin–Lattice Relaxation in the Rotating Frame

Another property that is routinely measured in the study of relaxation and dynamics is the spin-lattice relaxation in the rotating frame, $T_{1\rho}$ [60]. Experimentally $T_{1\rho}$ is measured by rotating the longitudinal magnetization to the transverse plane by the means of a $\pi/2$ pulse with subsequent application of a low amplitude pulse with the same phase as the resulting transverse magnetization, for the duration of τ (Fig. 23). This second pulse is referred to as the spin-locking pulse, or field, and is applied on the order of milliseconds, as opposed to microseconds for ordinary $\pi/2$ pulses.

If the power of the locking pulse is large enough the magnetization remains locked along the axis corresponding to the phase of the locking pulse and decays according to a 'T_1 like' process governed by the timescale of the locking

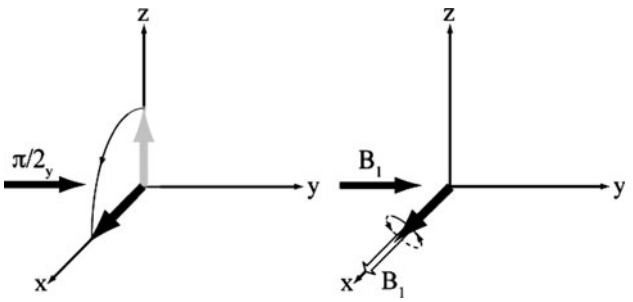

Fig. 24 Magnetization vector in the spin-lock experiment

power and not the Larmor frequency. After the locking period, τ, B_1 is turned off, releasing the transverse magnetization, which precesses freely and is detected. The behavior of the magnetization vector during the spin-lock experiment is illustrated schematically in Fig. 24.

The magnetization decays in the spin-locking frame as a function of τ and follows:

$$M_x = M_0 e^{-\frac{\tau}{T_{1\rho}}} \tag{19}$$

By measuring intensities of the decaying signal at different spin-lock times, the time constant of the process, $T_{1\rho}$, can easily be obtained. As $T_{1\rho}$ is sensitive to the timescale of B_1, it is also very sensitive to slow molecular dynamics that are usually inaccessible by conventional T_1 and T_2 measurements [61].

2.10 Cross-Polarization

Nuclei with small γ's and low natural abundance (^{13}C, ^{15}N, etc.) give weak NMR signals. Nuclei of this type also tend to have long T_1's requiring lengthy relaxation delays (10s to 1000s) [62]. In order to improve the signal-to-noise ratio of such spectra, either isotopic enrichment of the material or long experimental times are required, both of which are extremely expensive and often impracticable. These problems can be circumvented by using cross-polarization (CP), which involves magnetization transfer from an abundant strong nucleus to the rare weak nucleus of interest [63]. CP employs the flip-flop transitions, the mutual 'up-down/down-up' transitions that normally occur between strongly homonuclear coupled spins, and hence are not significantly active between rare nuclei. Heteronuclear flip-flop transitions can be re-induced during simultaneous spin-locking of an abundant spin **I** and a rare spin **S** under conditions that equalize their precession frequencies. CP establishes a new equilibrium in spin polarizations via the flip-flop transitions as determined by the ratio of their magnetogyric ratios:

$$\frac{P_{0I}}{P_{0S}} = \frac{\gamma_I}{\gamma_S} \tag{20}$$

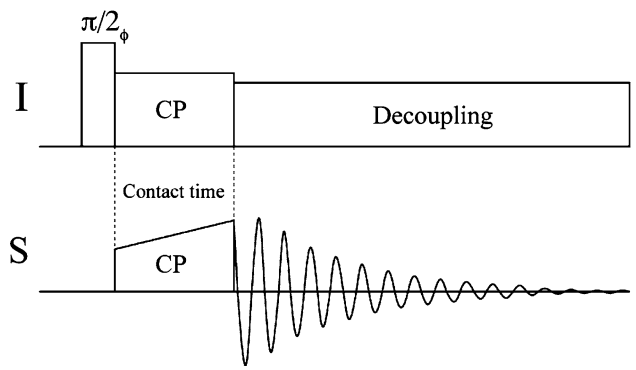

Fig. 25 Pulse sequence of an MAS NMR experiment with Hartmann-Hahn polarization transfer from abundant spin **I** to rare spin **S**

In principle, $^1H \rightarrow {}^{13}C$ cross-polarization can give an enhancement factor of 4.

CP transfer from spin **I** to spin **S** is established by first creating a transverse magnetization from spin **I**, via a $\pi/2$ RF pulse with an appropriate phase, followed by applying spin-locking fields B_{1I} and B_{1S} to both spins simultaneously, along the direction of the magnetization of spin **I**. The spin locking powers on both channels must meet the Hartmann–Hahn condition ($\gamma_I B_{1I} = \gamma_S B_{1S}$), thereby equalizing both spin frequencies ($\omega_{1I} = \omega_{1S}$), allowing for cross-polarization to take place and leading to the build-up of **S** magnetization along the B_1 axis during the contact period. When the spin-lock terminates on both channels it is followed by simultaneous detection of spin **S** and decoupling of spin **I**, as shown in Fig. 25.

The optimum duration of the spin-lock period, referred to as contact time, is determined by the $T_{1\rho}$ of spin **I**. The rate of polarization transfer, k_{IS}, is a complex function of the dipolar couplings between the two spins. The dynamics of the **I** → **S** CP is characterized by $T_{1\rho}$ and k_{IS} as shown in the CP curves of Fig. 26.

The magnetization of an abundant spin decreases exponentially with contact time, at a rate of $1/T_{1\rho(I)}$, while that of the rare spin grows at a rate determined by k_{IS}, reaching a maximum and subsequently decaying at a rate determined by $T_{1\rho(I)}$.

The development of cross-polarization techniques revolutionized modern NMR spectroscopy for solids and made it suitable for routine application. CP provides a many-fold enhancement of the signal to noise ratio for weak nuclei on a per scan basis. In addition, it allows for a faster scanning rate as it is limited by $T_{1(I)}$ rather than $T_{1(S)}$, which is always longer, often by orders of magnitude. As a result, the signal to noise ratio over a fixed experimental duration is improved dramatically. In CPMAS, CP is combined with MAS, offering both vastly improved resolution and greatly increased signal to noise, making it possible for SSNMR to become a routine technique in materials science.

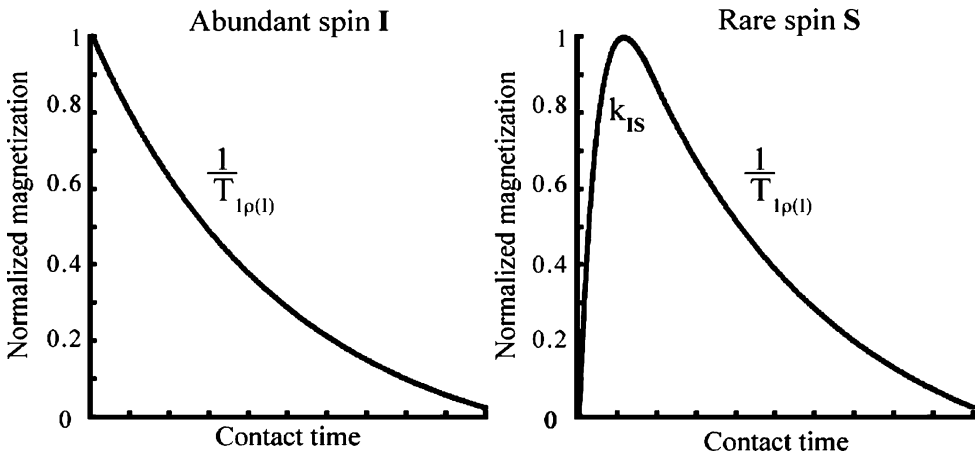

Fig. 26 Dynamics of polarization transfer from an abundant spin **I** to rare spin **S**

2.11 Multi-Dimensional NMR

In conventional one-dimensional (1D) NMR experiments, spin coherence created during the experiment is observed as a function of one time variable and the corresponding spectrum is constructed by plotting signal intensity as a function of one frequency variable. This approach is very limiting, as much information can be obtained by observing the spin system evolving over time. Furthermore, analyses of NMR spectra can be a near impossible task for large and complex molecular structures, as one-dimensional spectra can become hopelessly crowded and extremely difficult to interpret. Such spectra can be significantly simplified with multidimensional NMR spectroscopy, where the signal is detected as a function of several time variables. Two dimensional (2D) NMR experiments allow the observation of correlations between peaks in the spectrum due to spin–spin interactions that can be controlled using RF pulses. This provides detailed insight into connectivity between spins, inter- and intramolecular distances and molecular structures of both liquids and solids. Two-dimensional methods are composed of a series of specific experimental operations performed during each of four time periods: preparation, evolution, mixing and detection, as outlined in Fig. 27.

During the preparation phase spin coherence and transverse magnetization are created, normally with a 90° RF pulse or polarization transfer from another nucleus from a system that was allowed to return to equilibrium beforehand. Spins are subsequently allowed to freely precess at their Larmor frequency during the evolution period, t_1. Sometimes the system is subjected to decoupling sequences during this time. Additional operations performed on a spin system during the mixing period cause magnetization transfer between spins according to a chosen mechanism determined by the pulse sequence and normally allow for the establishment of coherences via through-space or through-bond spin–spin interactions. Ultimately, by the end of the mixing period a detectable coherence is created on the nucleus of interest. The pulse sequence ends with the detection period, during which the signal is observed as a function of a second time variable, t_2, often under decoupling conditions.

The value of t_1 is incremented, and the sequence is repeated for each point in the indirect time dimension, thereby creating an array of FIDs that constitute a data set that is two-dimensional in time S (t_1, t_2). This signal is then converted from time domains to the corresponding frequency domains, F_1 and F_2, via double Fourier transformation. Finally, the 2D spectrum is displayed as a contour map plot with frequency axes labeled F_1 and F_2, with correlations between the spins shown as a vertical projection of signal intensities and the peak coordinates reflecting respective frequencies. A basic two-dimensional correlation spectrum of an AX spin system is depicted in Fig. 28.

In one-dimensional NMR experiments, the corresponding FID of an AX spin system contains two signals, upon which Fourier transformation gives rise to two peaks

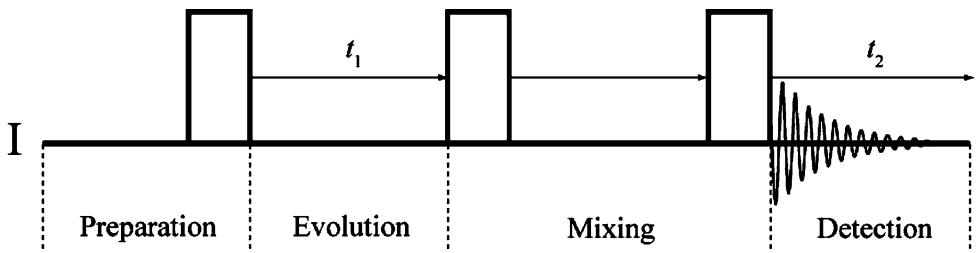

Fig. 27 A general pulse sequence diagram of a 2D NMR experiment

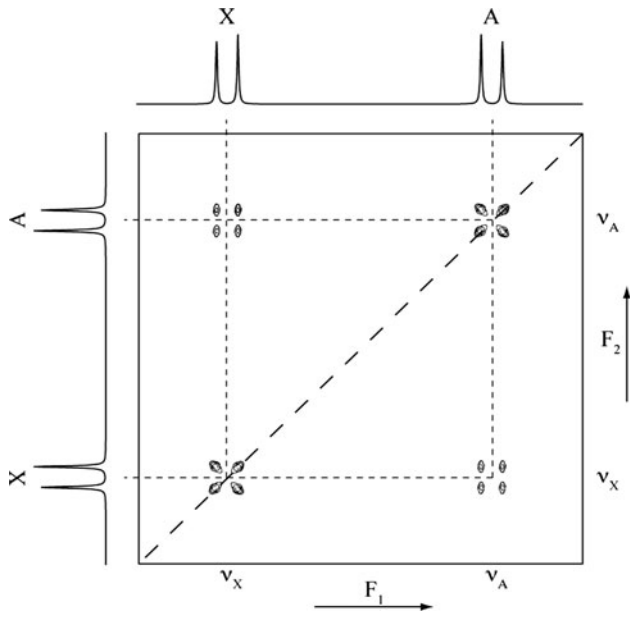

Fig. 28 2D correlation spectrum of an AX spin system

appearing at ν_A and ν_X, each of which are split into doublets due to *J*-coupling. The 2D correlation spectrum of this spin system exhibits two groups of peaks along the diagonal at (ν_X, ν_X) and (ν_A, ν_A) which show homonuclear correlations for spin X and A, respectively. Two off-diagonal sets of peaks, referred to as cross-peaks, characterize the homonuclear magnetization transfer that occurred between the coupled spins and therefore provide information about their connectivity, and often, relative geometry.

A basic two-dimensional NMR experiment can be designed by making modifications to the pulse sequence that enable specific coherence transfer to occur through a desired coherence mechanism [64–68]. Two-dimensional MAS NMR experiments also eliminate the necessity of windowed detection which is often used in advanced homonuclear decoupling methods such as FSLG [52], PMLG [55] and DUMBO [49].

One example of a routinely used two-dimensional MAS NMR experiment is the Incredible Natural Abundance Double Quantum Transfer (INADEQUATE) technique [69]. It leads to discrimination between signals from *J*-coupled spin pairs and isolated spins, where the latter can be eliminated through a series of pulses executed in a two-step phase cycle. Originally developed as a solution NMR technique [38], it was later adapted for solids under MAS conditions. During the preparation period, a spin echo sequence is applied, $\pi/2_x - \tau - \pi_y$, resulting in anti-phase magnetization on both spins in the spin pair which is converted to a double quantum coherence by the subsequent $\pi/2_x$ pulse. At this point the magnetization from isolated spins ends up along the $-z$ axis. The double quantum coherences evolve during t_1 according to the sum of chemical shifts only, as they do not evolve under *J*-coupling. The next $\pi/2_{x/y}$ pulse causes these double quantum coherences to be converted into single quantum anti-phase magnetization, although this time on the other spin in the spin pair, thus completing the coherence transfer process. The phase of this $\pi/2$ pulse is cycled between two successive acquisitions so that only the anti-phase magnetization can be detected; however, in order to allow for decoupling, it needs to be converted to in-phase magnetization, via application of a τ–π–τ refocusing pulse. Correspondingly, this experiment is referred to as the Refocused INADEQUATE; the pulse sequence is shown in Fig. 29. The INADEQUATE experiment applied to polymeric systems provides detailed information about bond connectivity between various structural features within the material (as seen in Fig. 30).

In heteronuclear correlation spectroscopy the coherence transfer between two nuclei of interest is often compromised by spin diffusion. As the name suggests, spin magnetization experiences diffusion-like processes across an entire spin system, due to mutual flip-flop transitions occurring between homonuclear dipolar coupled spins. Under modest spinning conditions, homonuclear dipolar couplings often remain strong in experiments involving abundant nuclei with large magnetic moments. This results in efficient magnetization exchange due to spin diffusion giving rise to non-unique crosspeaks that are problematic in establishing connectivity. Fortunately, spin diffusion can be efficiently suppressed by using either FSLG/PMLG [52, 55] homonuclear decoupling, or by using ultra-fast spinning (70 kHz).

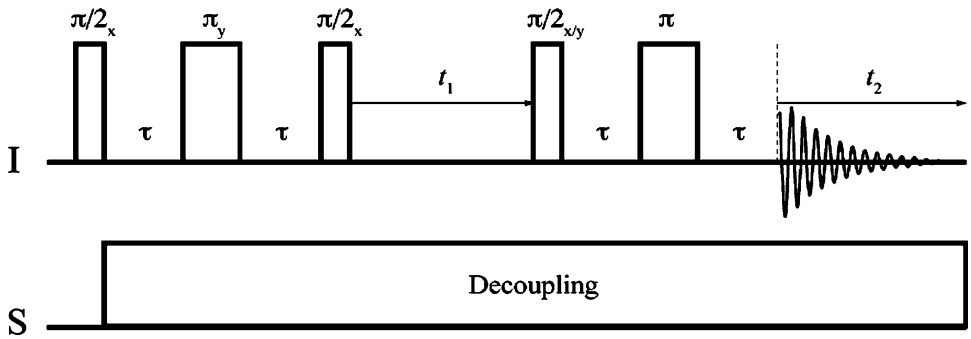

Fig. 29 Pulse sequence of the two-dimensional refocused INADEQUATE MAS NMR experiment

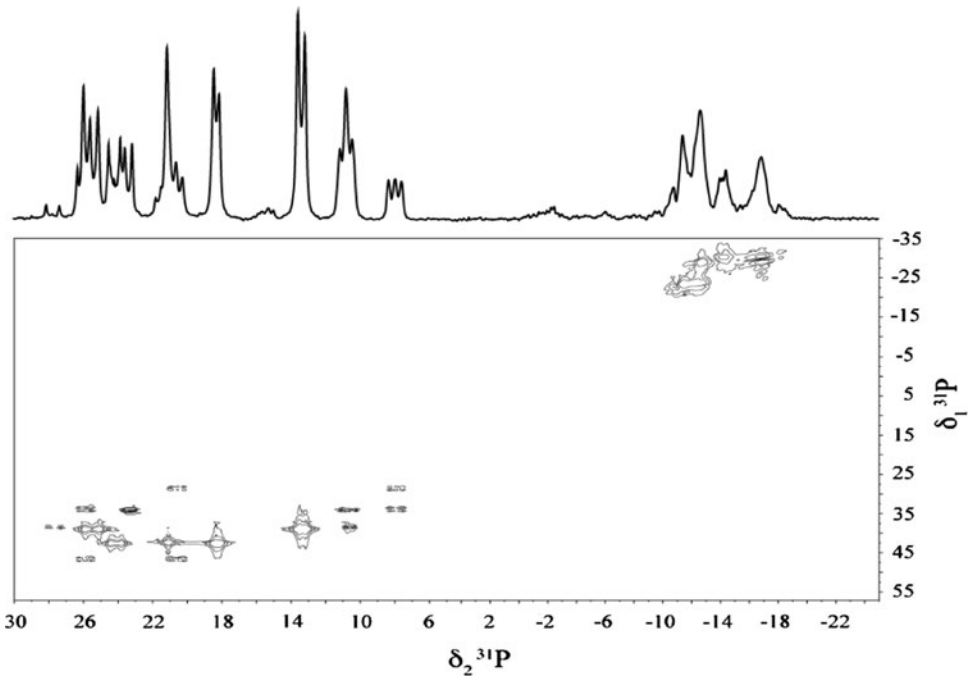

Fig. 30 Two-dimensional 202 MHz ^{31}P—^{31}P refocused INADEQUATE MAS NMR spectrum of the partially trifluoroethoxy-substituted poly(dichlorophosphazene). MAS rate 10 kHz

2.12 Recoupling Sequences

As mentioned earlier, dipolar coupling can be effectively averaged out under MAS conditions in solid-state NMR; however, in some cases this coupling information is desired to measure internuclear distances or to simply establish connectivity for molecular structure elucidation. A number of experiments allow dipolar interactions to be reintroduced by the application of a series of RF pulses during an evolution period and are referred to as dipolar recoupling sequences [70–74].

One of the best known recoupling experiments is the Rotational Echo Double Resonance (REDOR), first introduced by Schaefer and Gullion [75]. The REDOR sequence is composed of two π pulses applied per rotor period on spin ***S***, which prevents the ***I***–***S*** dipolar coupling from being fully refocused at the end of each full rotation and leads to dephasing of the transverse magnetization under the ***I***–***S*** dipolar coupling. The intensity of spin ***I*** is then compared with intensity of spin ***I*** in the reference experiment, where no pulses are applied on spin ***S***. This difference is plotted as a function of rotation periods, which corresponds to the distance axis for dipolar interactions of different magnitudes. The REDOR sequence is commonly used to measure interatomic distances in the range of 2–8 Å [76–78].

For a strongly dipolar-coupled spin pair it is possible, in principle, to create a double quantum coherence. Through a series of radio-frequency pulses a double-quantum coherence between two spins can be excited and subsequently allowed to evolve under dipolar coupling. One the most commonly used experiments for exciting the double quantum coherence is the BABA sequence [79, 80]. BABA has proven very effective for exciting homonuclear multiple quantum coherences with a basic pulse sequence being composed of 90° pulses placed back-to-back: ($\pi/2_x - \tau_r/2 - \pi/2_{-x} - \pi/2_y - \tau_r/2 - \pi/2_{-y}$). Double quantum coherence is then converted to an observable single quantum coherence and the signal intensity is measured as a function of excitation time. Such sequences, which are referred to as double quantum filters (DQF), provide information about the dipolar coupling between two spins, from which spatial configuration and proximity at the atomic level can be determined. BABA is also commonly used in heteronuclear correlation experiments, where the double-quantum coherence between two different spins is created by applying a pulse sequence on both spin channels simultaneously. These sequences are usually a part of a two-dimensional experiment and allow for measuring homonuclear and heteronuclear dipolar couplings.

Another example of a two-dimensional dipolar recoupling experiment is the Radio-Frequency Driven Recoupling (RFDR), where mixing of the longitudinal magnetizations is achieved using a series of rotor-synchronized π pulses that interfere with the averaging of the dipolar coupling under MAS conditions [81, 82]. This reintroduces dipolar coupling causing longitudinal spin polarization to exchange, leading to correlation between spins with different chemical shifts that are dipolar-coupled. The sequence terminates with a $\pi/2$ pulse converting the longitudinal magnetization back to the transverse coherence which is detected. A pulse sequence diagram for the RFDR experiment is shown in Fig. 31. The

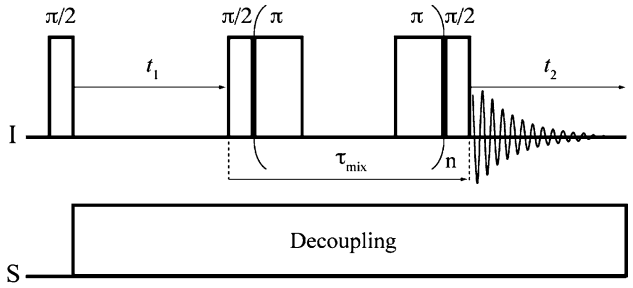

Fig. 31 Pulse sequence of the two-dimensional RFDR MAS NMR experiment

corresponding 2D spectrum contains cross-peaks between dipolar-coupled spins, from which intramolecular connectivity are determined.

Dipolar couplings between spin-1/2 and quadrupolar nuclei can be measured using Transfer of Population in Double Resonance (TRAPDOR) [83–85] or 'Rotational-Echo, Adiabatic Passage, Double Resonance' (REAPDOR) [86–89] experiments.

The TRAPDOR experiment is applied to spin-1/2—quadrupolar spin pairs under MAS conditions. In this method the Zeeman energy level populations of the quadrupolar nucleus are changed during the rotor period by applying a continuous radio-frequency pulse for half of the dephasing period. The strength of the quadrupolar interaction depends on molecular orientation with respect to the external magnetic field, which under MAS conditions changes constantly. This prevents dipolar coupling between spin-1/2 and quadrupolar nuclei from being averaged out and can be used for determining average internuclear distances [83–85].

Other examples of recoupling sequences include Dipolar Recovery at the Magic Angle (DRAMA) [90], Transferred Echo Double Resonance (TEDOR) [91, 92], and the numerous symmetry-based sequences introduced by Levitt et al. (C_n^N and R_n^N) [50, 93–101].

Recoupling sequences have already proven extremely useful for determining internuclear distances and connectivity in a variety of materials (as will be shown by several examples of applications for inorganic polymers), and will likely form a main approach in multi-dimensional correlation methods in solid-state NMR spectroscopy.

3 Applications of Solid-State NMR Methods in Polymers

3.1 Molecular Structures and Connectivity in Polymers

NMR spectra of polymers consist of superimpositions of peaks from numerous and often diverse macromolecular environments. In principle, provided that sufficient resolution can be achieved, accurate determination of chemical shifts, widths, intensities, composition (via deconvolution analysis), and connectivity can lead to the elucidation of 'average' local atomic structures of the recurring units, side-chains and defects. Furthermore, the signal from chain-end groups can be compared to those corresponding to the main chain to determine its length in terms of the number of repeating units, and thus, provides an estimate of the average molecular weight. Similar comparison can be made to determine the degree of cross-linking in the polymer if a characteristic signal can be identified. Variable temperature experiments often exhibit changes due to phase transitions in the polymer. This not only indicates that a phase transition is occurring but also identifies the process at the molecular level; therefore, MAS NMR is invaluable in the study of polymer morphology and thermochemistry.

Detailed information about the molecular structure, cross-linking and backbone and side-chain geometry of polymers can be determined from through-space and through-bond connectivity primarily by two-dimensional MAS NMR experiments. A variety of such 2D solid-state NMR techniques exist today and are routinely used in the study of materials [102–105]. Two examples of such work include the study of the P–O–P connectivity in crystalline and amorphous phosphates using the 2D INADEQUATE pulse sequence [106–108], and determination of through-space heteronuclear connectivity in polymers using HETCOR spectroscopy [9, 109–124]. Several other two-dimensional solid-state NMR experiments have recently been developed that can provide information about structures of materials, such as: Insensitive Nuclei Enhancement by Polarization Transfer (J-INEPT) [125–127], Heteronuclear Multiple-Bond Connectivity (HMBC) [128], Through-bond Heteronuclear Single-quantum Correlation (MAS-J-HSQC) [129] and Through-bond Heteronuclear Multiple-quantum Correlation (MAS-J-HMQC) [130]; however, they suffer from self-cancellation of signals in systems with broad lines (common to polymers) caused by inhomogeneity of the phase of magnetization requiring refocused methods.

Solid-state NMR spectroscopy can be an excellent tool for establishing structures and connectivity in polymers at the molecular level, which in turn relates to their macroscopic properties and applications. MAS NMR can be applied to a broad array of polymers, regardless of their solubility, crystalline/amorphous composition and many other parameters that often limit the application of other conventional spectroscopic methods. Several examples given in the aforementioned paragraph demonstrate the versatility and usefulness of solid-state NMR for

determining structures and inter-nuclear distances in various polymers.

3.2 Molecular Dynamics of Polymers

Molecular dynamics can have a profound impact on important properties of a polymer, such as flexibility, elasticity and permeability. Unlike solutions where rapid molecular motions largely average out the orientationally dependent spectral parameters, in solids, relaxation, linewidths and dipolar interactions, which strongly depend on molecular motion, can provide detailed insight into chain dynamics. Solid-state NMR spectroscopy is a very powerful tool for probing chain dynamics within polymers, in both amorphous and crystalline domains [131]. Most common techniques used to elucidate segmental motion in polymers, depending on the timescale of molecular interactions, include measurements of T_1, T_2 and $T_{1\rho}$ relaxation [11, 117, 132–139], lineshape analysis [140–143], cross-polarization dynamics [24, 120, 144, 145] and advanced two-dimensional experiments [146–151].

Information about dynamic processes is readily accessible via measurement of spin relaxation. Recall that the spin magnetization experiences relaxation processes due to the constant perturbations from local time-dependent magnetic fields, which are caused by CSA, spin–spin couplings and other orientationally dependent interactions that are modulated by nearby molecular motion. The motion of these fields is characterized by the correlation time, τ_c, and must be near the Larmor frequency of the nucleus in order for relaxation to occur: $\tau_c \approx 1/\omega_0 \approx 10^6$–$10^9$ Hz. Since dynamics in solids is several orders of magnitude slower than in liquids, it is desirable to enable detection of motions at slower frequencies. Hence, a common approach in MAS NMR is to measure $T_{1\rho}$, which is determined by the strength of the spin-lock field, (several kHz; $T_{1\rho} \approx 1/\omega_1 \approx 1$ ms to 10 μs), rather than the magnetic field strength, (100s of MHz). The closer $1/\tau_c$ is to the spin locking frequency of the nucleus, the faster the relaxation rate will be. In fact, the rate reaches a maximum when the two are equal. Correlation times are temperature dependent, and thus, obey the Arrhenius form. Therefore, one can measure relaxation as a function of temperature and extract the rate of motion from the maximum in the plot of $1/T_x$ vs. T where T_x is T_1, T_2 or $T_{1\rho}$. This approach is widely utilized for elucidating quantitative information about dynamic processes at specific sites of bulk organic, inorganic and biological polymers [15, 152–161].

As discussed previously, solid-state NMR spectra consist of powder patterns composed of individual lines that correspond to different molecular orientations with respect to an external magnetic field. These lines overlap and give rise to structural features in an observable signal. Molecular dynamics and exchange processes that cause a molecule to reorient with respect to a magnetic field will result in a frequency shift of the corresponding line in the spectrum. If the rate of such reorientations is on the same timescale as the width of the powder pattern (10^3–10^4 Hz), this will lead to distortions in the latter that are dependent on the correlation time and geometry of the molecular motion. Consequently, information about molecular motion can be assessed via lineshape analysis [140–143, 162, 163].

Dynamic processes in solid materials are also commonly studied using lineshape analysis of ^{2}H spectra, whereby linewidths in the powder pattern are observed as a function of temperature to reveal details about correlation times and molecular dynamics [164].

A common approach to investigating slow dynamics in solids under MAS conditions utilizes two-dimensional Exchange Spectroscopy (EXSY) [131] and Centerband-Only Detection of Exchange (CODEX) [165], in which the chemical shift anisotropy is recoupled under MAS conditions through a series of rotor-synchronized pulses leading to the longitudinal magnetization exchange between nuclei. In the absence of exchange the magnetization is refocused; however, refocusing can be compromised when motion is present during the mixing period. Through analysis of line intensities as functions of mixing time and rotor period it is possible to determine the rate and range of molecular motions occurring at much lower frequencies (10^{-1}–10^4 Hz). Such information is particularly useful for investigating very slow dynamics of polymers near glass-transition temperatures. A recent example is the ^{31}P CODEX study of anion dynamics in a series of benzimidazole-alkyl phosphonate salts [22].

In solids, molecular dynamics in polymers can be readily determined by measuring relaxation, lineshapes and couplings. There is now a collection of techniques available that make it possible to obtain information about dynamic processes occurring at a broad motional range, with timescales from microsecond (bond rotations) to days (thermodynamic transitions), covering ten orders of magnitude. Application of these methods to inorganic polymers could prove invaluable, giving insight into the effect motion at the atomic scale has on macroscopic properties of a material, such as flexibility, elasticity, permeability, etc.

3.3 Domains and Phases of Polymers

In order to fully understand the macroscopic properties of polymers, it is necessary to obtain detailed information about various crystalline, amorphous and interfacial environments, such as size, morphology and phase structure. These aspects of the domains would be more easily studied if it were possible to investigate them separately. Domain

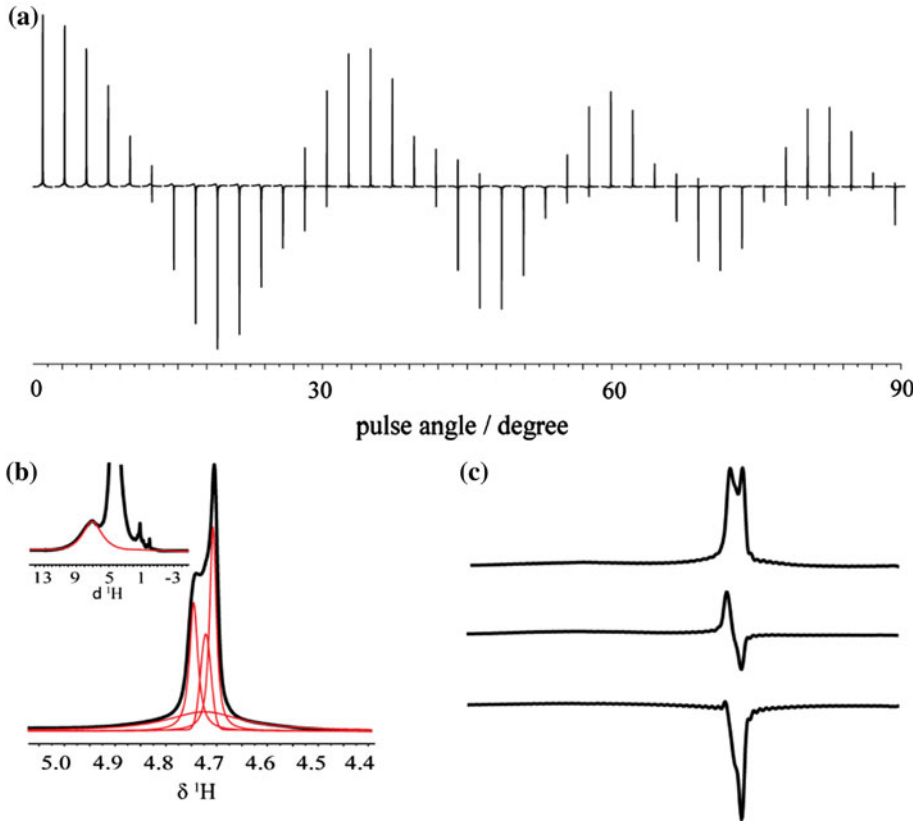

Fig. 32 **a** The 500 MHz ^{1}H MAS NMR direct DIVAM nutation experiment on solvent-cast PBFP. MAS rate 25 kHz; **b** the deconvolved ^{1}H MAS NMR spectrum of solvent-cast PBFP showing multiple overlapping components; **c** expansions of the array at the mini-pulse angles of 9°, 10.8° and 12.6° showing individual components crossing zero at slightly different angles

selective methods have been developed for MAS NMR for just that purpose, and have proven to be very effective in probing such properties [13, 30, 32, 33, 166–169]. Efficient domain selection is made possible through filtering the signals on the basis of differences in relaxation rates, dipolar interactions and CSAs. This makes it possible to perform spin diffusion measurements which are used to determine domain sizes.

Relaxation-based sequences exploit differences in T_1, T_2 and $T_{1\rho}$ which are normally significantly shorter in ordered crystalline environments. Therefore, the pulse sequence can be set up so that only the signals from amorphous domains remain behind [170]. Differences in the strengths of dipolar interactions can be used to selectively remove domains with strong dipolar interactions [171]. This, again, would give rise to sequences that are selective for mobile amorphous domains. Sequences that utilize this approach are pulse saturation transfer [172], dipolar filter [173], dipolar dephasing [174–177], cross-polarization–depolarization [178–180] and Discrimination Induced by Variable Amplitude Minipulses (DIVAM) [181–185] MAS NMR experiments. The DIVAM sequence is particularly versatile as it can be tuned to select amorphous or crystalline signals on the basis of relaxation (T2) or coherent spin dynamics (CSA, isotropic chemical shift, and dipolar coupling), within one experiment. A typical direct DIVAM experiment used to select the signals of interest is illustrated in Fig. 32. It was further modified to remove resonance offset effects turning it into a CSA-based filter and removing phase distortions. Other chemical shift anisotropy techniques have also proven useful for discriminating between different polymer domains [172, 186].

As previously discussed, spin diffusion reflects structural and dynamic features of different domains of the bulk material. Selective excitation of a particular domain in the polymer, followed by subsequent monitoring of the change in the signal for each domain over time, allow the determination of the spin diffusion rates. From this, one can estimate the average distance over which the diffusion process takes place, which indicates the size of the domains. Since this process is influenced by the heterogeneity of polymer environments, spin diffusion measurements make it possible to obtain unique insights into polymer morphology, surface and interfacial properties, domain structures and sizes, and the miscibility of polymer and polymer blends [187–196]. Two of the most commonly used techniques based on the observation of spin diffusion include the Goldman–Shen-based experiments [197] and 2D WISE spectroscopy [198–201].

MAS NMR spectroscopy offers a wide variety of techniques for investigating polymer phases and domains. It has been successfully applied to inorganic polymeric

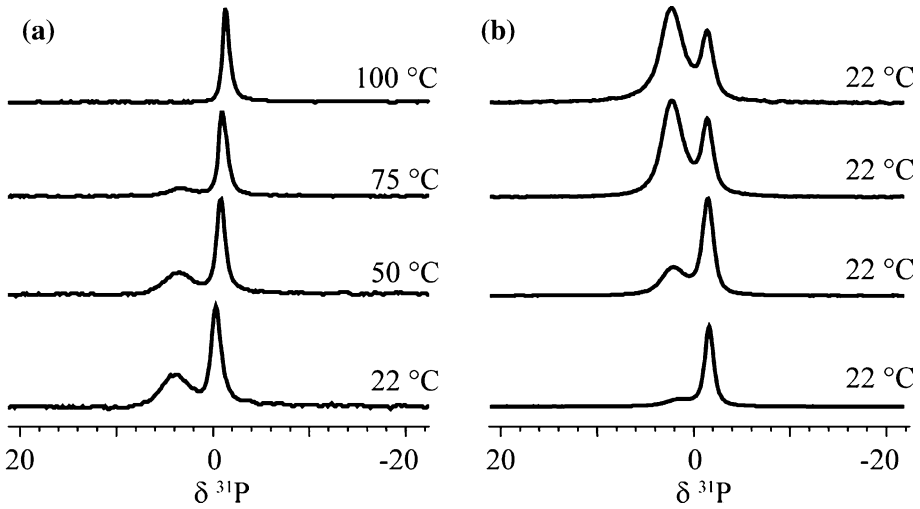

Fig. 33 **a** ^{31}P MAS NMR spectra of PBFP at various temperatures during heat treatment. The spectrum at room temperature contains a sharp peak due to the amorphous phase and one broad peak due to crystalline phase. As the temperature is increased above thermotropic transition T(1) only the signal from mobile mesophase is observed; **b** The ambient temperature ^{31}P MAS NMR spectra of PBFP after being subjected to several heat cycles. The bottom spectrum represents virgin PBFP cast from acetone, while the top spectrum shows PBFP after 11 cycles of heat treatment. A continuous enhancement of the crystalline phase is observed with each cycle

systems in the past [1, 7, 13, 30, 32, 33, 166–170, 172, 173, 194–196, 202], providing valuable morphological information, such as shown in Fig. 33. Solid-state NMR methods can help establish how synthetic preparations affect the phases and domains within polymers which gives control over the crystalline/amorphous composition for specific applications. This information is often either hard to obtain or inaccessible via other spectroscopic methods routinely used today, making MAS NMR spectroscopy a truly unique and invaluable tool.

4 Inorganic Polymers

4.1 Overview

Inorganic polymers can be classified as fully inorganic (i.e. entirely comprised of inorganic elements), organic–inorganic hybrid, or organometallic. They offer a number of significant advantages, such as increased chemical resistance, thermal stability and mechanical durability. The unique composition of inorganic polymers efficiently reduces problems arising from aging, degradation, toxic fume emission upon ignition, etc., usually associated with organic polymers. A variety of elements found in the backbone and side-chains allows tailoring of chemical and physical properties of the polymer to suit specific applications, which can range from very basic to high-performance, such as electronics components and biomedical materials [203, 204]. In addition, the relatively low cost of mass-production of polymer materials and the mild conditions under which they can be processed into usable products renders them more commercially valuable than conventional materials with similar properties, such as metals.

Ultimately, inorganic polymers comprise a rapidly growing field of material science, where materials with unique properties and new applications are constantly being developed and reported [203, 204]. The following sections will review structures, syntheses, basic properties, applications and examples of solid-state NMR characterization of the most commonly studied and utilized classes of inorganic and organometallic polymers.

4.2 Silicon-Based Polymers

4.2.1 Polysilanes

Polysilanes are a promising class of inorganic polymers and are composed of a linear backbone of continuous silicon atoms. They were first synthesized by Kipping in 1921 [205], and are most commonly obtained today via either condensation reactions or ring-opening polymerization [206]. A general structure of the repeating polysilane unit is shown in Fig. 34.

Fig. 34 General structure of polysilanes

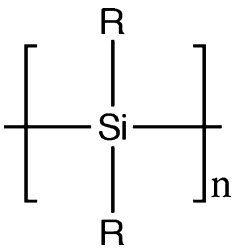

Typically, polysilanes have relatively low glass transition temperatures, and their physical properties depend on the functionalities in the side-chains. Polymers with small, identical side-chain groups, such as CH_3, tend to be highly crystalline and insoluble solids; however, the crystallinity decreases in cases with units of larger size or when dissimilar groups are attached to the Si backbone. Polysilanes exhibit unique behavior due to σ-delocalization in the Si–Si bonds [204], which gives rise to useful properties, such as electro- and photoconductivity, photosensitivity and long wavelength UV absorption. The most interesting applications of such materials include semiconductors, non-linear optical materials, photoconductors and photoresistors [204, 207]. Polysilanes with pendent metal complex segments were found to be useful in the area of new organic electroconductive materials [208, 209]. Modification of the backbone of soluble polysilanes by interrupting the Si–Si sequence with a carbon atom yielded pre-ceramic polymers that could be turned into usable silicon-carbide (SiC) ceramic materials through pyrolysis or chemical vapor deposition [210].

In the past, solution-state NMR spectroscopy has been used extensively to elucidate chemical structures and polymerization mechanisms of various polysilanes [207, 211–222]. In contrast, solid-state NMR methods were primarily employed to obtain information about conformation, phase transitions and morphologies of polysilanes [222].

Solid-state ^{13}C and ^{29}Si NMR spectra of oligomeric perphenylpolysilanes were published in 1985 and indicated the presence of multiple molecular environments [223]. The conformation of poly(methylphenylsilane) and poly (dimethylsilyldiphenylsilane) was probed using ^{29}Si CPMAS SSNMR spectroscopy over a range of temperatures [224, 225]. SSNMR was also used to probe the trans chain dynamics of poly(dimethylsilylene), which was established to be more rigid than the diethyl homologue [226].

Poly(di-*n*-propyl-silylene) and poly(diethylsilylene-co-di-*n*-propylsilylene) were extensively characterized using TGA, DSC, X-ray diffraction, Raman, IR, UV and solid-state ^{13}C and ^{29}Si NMR spectroscopy [227]. The transformation of polysilane to polycarbosilane during the pyrolysis of poly(methylchlorosilanes) was studied by ^{13}C and ^{29}Si cross-polarization and inversion recovery cross-polarization MAS NMR which provided the opportunity to observe various silane and carbosilane sites [228, 229]. Phase transitions and backbone conformations of poly (dimethylsilane), poly(diethylsilane), their copolymers and poly(ethylmethylsilane) were observed using ^{29}Si CPMAS NMR [230].

Solid-state ^{2}H quadrupolar echo and two-dimensional exchange experiments at variable temperatures were applied to investigations of segmental mobility in poly(methylphenylsilane) revealing fractions with fast, intermediate and slow motions, which were assigned to amorphous, interfacial and crystalline domains, respectively [231]. ^{2}H and ^{29}Si solid-state NMR spectroscopy was used to study the phase behavior of poly(di-*n*-decylsilane) and its deuterated derivative. The results, which were consistent with DSC data, indicated the presence of two crystalline environments within the polymers [232].

4.2.2 *Polysiloxanes*

Polysiloxanes, commonly known as silicones, consist of a backbone of repeating siloxane (Si–O) units (shown in Fig. 35) and are found in a broad range of commercial products [206]. Depending on the functionality of the side-chains, polysiloxanes can be composed of either linear chains or cross-linked networks and can range from fluids to gels to elastomers to resins [233–236].

Relatively high Si–O bond strengths and increased Si–O–Si bond angles result in the thermal stability, extreme flexibility and high gas permeability enjoyed by polysiloxanes. Various structures of the side-chain units of the polymer define its physical properties and potential applications, which include membranes, high-voltage insulators, water repellents, adhesives, lubricants and ceramic composites. Biocompatibility, inertness and stability make silicones suitable for various medical applications, such as artificial organs and tissues, prostheses, contact lenses, cardiovascular devices, breast implants and devices preventing sexually transmitted infections [204, 234].

Several interesting studies of polysiloxanes using solid-state NMR spectroscopy have been reported. One interesting example is an investigation of the microphase structure of a series of poly(styrene-b-methylphenylsiloxane) copolymers [237]. Measurements of ^{1}H spin diffusion, combined with a dipolar filter and line-narrowing techniques, provided quantitative information about domain sizes and permitted the observation of an interphase in the phase-separated polymer systems.

Polysiloxane networks formed by copolymerization of tetraethoxysilane and dimethyl(diethoxy)silane were probed using ^{1}H and ^{29}Si spin–lattice relaxation in the rotating frame, as well as dipolar dephasing and spin diffusion

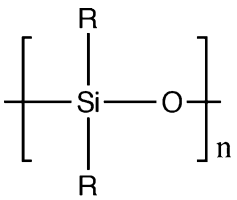

Fig. 35 General structure of polysiloxanes

NMR experiments. The combination of the resulting data revealed the heterogeneity of the system on the nano-scale [238].

Proton–silicon and proton–proton interatomic distances in hybrid polysiloxane networks were measured using CP dynamics, ^{1}H chemical shifts and WISE spectroscopy. Based on these results a structural model of the system was suggested [239].

Solid-state NMR spectroscopy can also provide useful information about hydrogen-bonding and surface morphology, as described in a study of polysiloxane networks [240]. Four different types of hydroxyl groups and the inhomogeneity of the hydrogen-bonding network were observed using ^{1}H CRAMPS experiments. Two-dimensional proton spin diffusion provided information about proton–proton distances, from which the average size of hydroxyl clusters was estimated. ^{1}H-^{29}Si heteronuclear correlation experiments facilitated the assessment of bond strengths of different hydroxyl groups within the siloxane network.

An interaction of Li^{+} ions and a crosslinked polysiloxanes matrix doped with lithium perchlorate was probed using ^{7}Li solid-state NMR lineshape analysis [241]. The temperature- and concentration-dependence of the chemical shifts was correlated to ionic conductivity.

4.2.3 Polysilazanes

Another important class of silicon-based polymers is polysilazanes, which contain a backbone of alternating Si and N, as depicted in Fig. 36 [206].

Polymers with only linear chain structures possess relatively low molecular weights (MW); however, species with high MW can be obtained by dehydrocoupling of oligomers. Polysilazanes are commonly used as precursors for silicon nitride ceramics, which are formed at high temperatures and provide heat and impact resistant materials [206, 242].

Most common polysilazane applications of solid-state NMR are focused on the characterization of structural changes upon the pyrolytic conversion of polysilazanes into ceramic products. The insolubility of ceramics and a variety of NMR-observable nuclei in their composition make them perfect candidates for solid-state NMR spectroscopy. In addition to ^{1}H, ^{13}C and ^{29}Si experiments used to elucidate structural changes upon ceramization and to identify pyrolysis residues in polysilazanes [243–249], several studies have demonstrated that ^{11}B, ^{15}N and ^{27}Al SSNMR can also be extremely useful for providing additional structural information [250–254].

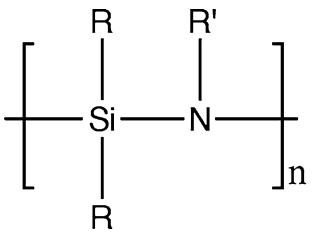

Fig. 36 General structure of polysilazanes

4.3 Metal-Containing Polymers

Polymers of this type contain a variety of main group metals, transition metals or rare earth metals in the repeating unit and comprise a very unique part of materials science. Numerous variations with metals incorporated directly in the backbone, or covalently bonded to the backbone, have resulted in novel and versatile materials which advantageously combine common properties of typical polymers with electrical, conductivity and redox properties of metals.

The most widely utilized polymers of this class are polymetallocenes, which are composed of repeating units of metals with two η^{5}-bound cyclopentadienyl ligands, as seen in Fig. 37.

In particular, polyferrocenes, which contain iron, exhibit useful and unique properties, and hence, are widely developed and characterized. Most of this work was pioneered by Abd-El-Aziz [255–258] and Ian Manners [259–261]. A general structure of a polyferrocene is shown in Fig. 38. Various applications of polyferrocenes include semiconductors, adhesives, antioxidants and lubricants [206].

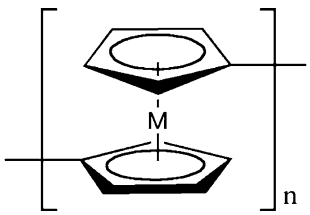

Fig. 37 General structure of a metallocene repeating unit

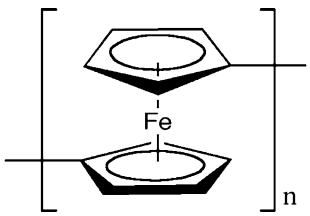

Fig. 38 General structure of a polyferrocene

Only limited information about solid-state NMR of polymetallocenes can be found in the literature. Kulbaba et al. [262–264] used ^{2}H solid-state NMR to examine molecular dynamics of a series of selectively deuterated poly(ferrocenylsilanes). Lineshape analysis provided insight into motions in the backbone and side-chains of polymers over a broad range of temperatures.

In a recent work by Widdifield and Schurko [265] polymeric potassium cyclopentadienide was characterized using ^{13}C and ^{39}K solid-state NMR spectroscopy. These experiments provided information about structure and temperature-dependent physical changes on the molecular level, and proved useful for identifying impurities in the system.

4.4 Polyphosphazenes

Polyphosphazenes are an important class of inorganic polymer that has been widely developed and studied in the past 30 years [203, 206, 266]. The backbone of the polymer consists of alternating phosphorus and nitrogen atoms, with two side chain units attached to each phosphorus (seen in Fig. 39).

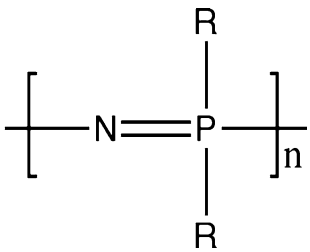

Fig. 39 General structure of polyphosphazenes (R = NHR, NHAr, OR, OAr, Ar)

The common approaches to obtaining poly(dichlorophosphazene) are the living cationic polymerization of phosphoroanimine ($Cl_3P = NSiMe_3$) at ambient temperature [267], thermal ring-opening polymerization (ROP) of hexachlorocyclotriphosphazene $(NPCl_3)_2$ [268, 269] and thermal condensation of $Cl_3PNP(O)Cl_2$ [270, 271].

Over 700 derivatives have been prepared from poly(dichlorophosphazene) via direct nucleophilic substitution of chlorine in the side units (Scheme 1) [266]. This variety of side chains provides materials with unique and useful properties. Most common applications of polyphosphazenes include, but are not limited to, artificial bone grafts, soft tissue prostheses, chemotherapeutic models, drug delivery systems, electrical devices, optical materials, membranes, and solid polymer electrolytes [203].

Apart from other major classes of inorganic polymers, polyphosphazenes have been widely studied and characterized using solid-state NMR spectroscopy, as will be shown with select examples.

The first notable polyphosphazene application of MAS NMR was reported in 1983 by Pratt Ackerman. In this manuscript ^{31}P solid-state NMR experiments were used to observe chemical shift anisotropies and molecular motion in several phosphazene elastomers [272]. Five years later, in 1988, Tanaka et al. [273] used multinuclear MAS NMR for investigating phase transitions in a representative poly[*bis*(4-ethylphenoxy)phosphazene]. This work was followed by variable-temperature ^{31}P experiments on poly[*bis*(trifluoroethoxy)phosphazene], from which the thermotropic transition temperature $T(1)$ was estimated [274].

A few years later the activation parameters for phenoxy group motion about the P–O bond, as well as the existence of interfacial regions, were determined for semicrystalline poly[*bis*(phenoxy)phosphazene] [275]. The morphology,

Scheme 1 Polyphosphazene derivatives obtained via nucleophilic substitution of side-chains in poly(dichlorophosphazene)

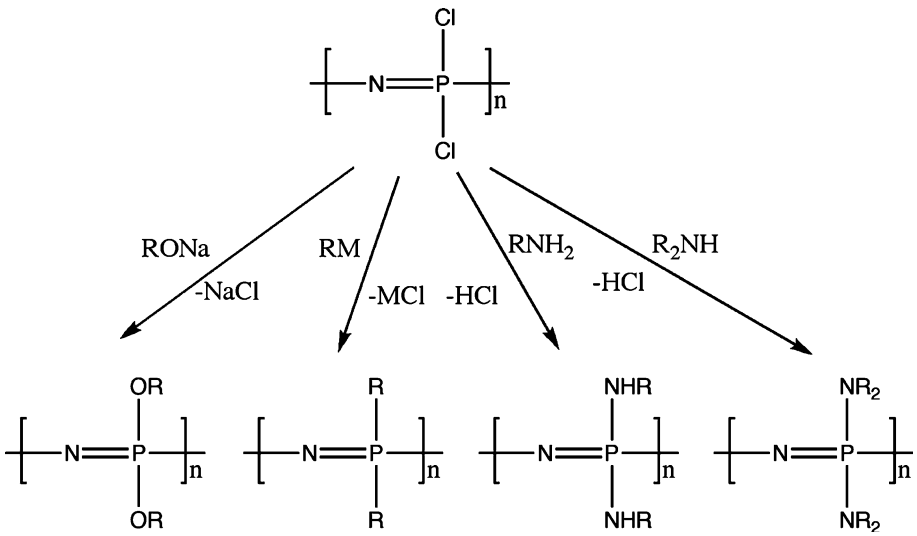

molecular dynamics and lamellar thickness of poly[*bis*(3-methylphenoxy)phosphazene] were probed using ^{1}H, ^{13}C and ^{31}P solid-state NMR experiments [195].

Simonutti et al. [276, 277] investigated morphology and side-chain mobilities of poly(diethylphosphazene) using variable-temperature ^{1}H–^{13}C–^{14}N triple-resonance MAS NMR experiments. Relaxation rate measurements and variable temperature solid-state NMR were used to probe dynamics of swelling and solvent permeation processes [278].

The DIVAM domain selection filter and high-resolution ^{1}H, ^{19}F, ^{31}P and ^{13}C fast-MAS NMR experiments were performed on poly[*bis*(trifluoroethoxy)phosphazene], where significant improvements in spectral resolution allowed for the preliminary assignment of signals from various crystalline, mesophase and amorphous regions of the polymer [32].

The backbone dynamics in deuterated poly[*bis*(methoxy)phosphazene] near its glass transition temperature T_g were probed using ^{2}H solid-state NMR spectroscopy [279]. Spin–lattice relaxation, lineshape and stimulated-echo methods were used to monitor changes in the segmental dynamics upon sample cooling over a broad temperature range. The results indicate that polymers with organic and inorganic backbones exhibit essentially the same segmental dynamic behavior during vitrification.

Finally, the most recent account in this area features ^{31}P MAS NMR spectroscopy of hexachlorocyclotriphosphazene at different stages during thermal ring-opening polymerization, as shown in Fig. 40 [280]. The spectra were collected at various stages during the course of polymerization (3, 8 and 17.5 h). The signals from trimer, oligomer and polymer species were identified and utilized to describe changes in the reaction mixture during polymerization. These results showed promise in making observations on the rates of chain propagation and cross-linking during thermal ring-opening polymerization.

5 Conclusion

We have reviewed a variety of solid-state NMR experiments that can be effectively used to characterize polymer systems. As shown in the previous sections, as far as solid-state NMR applications for inorganic polymers are concerned, the majority of studies are based on standard cross-polarization magic-angle spinning experiments. Advanced NMR techniques, such as heteronuclear correlation spectroscopy, double-quantum methods, domain selection filters, etc., all of which are routinely applied to organic and biological polymers, have not yet seen widespread use in inorganic analogues.

At this point advances in NMR instrumentation have removed many of the restrictions on the composition and state of the materials to which its methods can be applied. In addition, recent developments in pulse

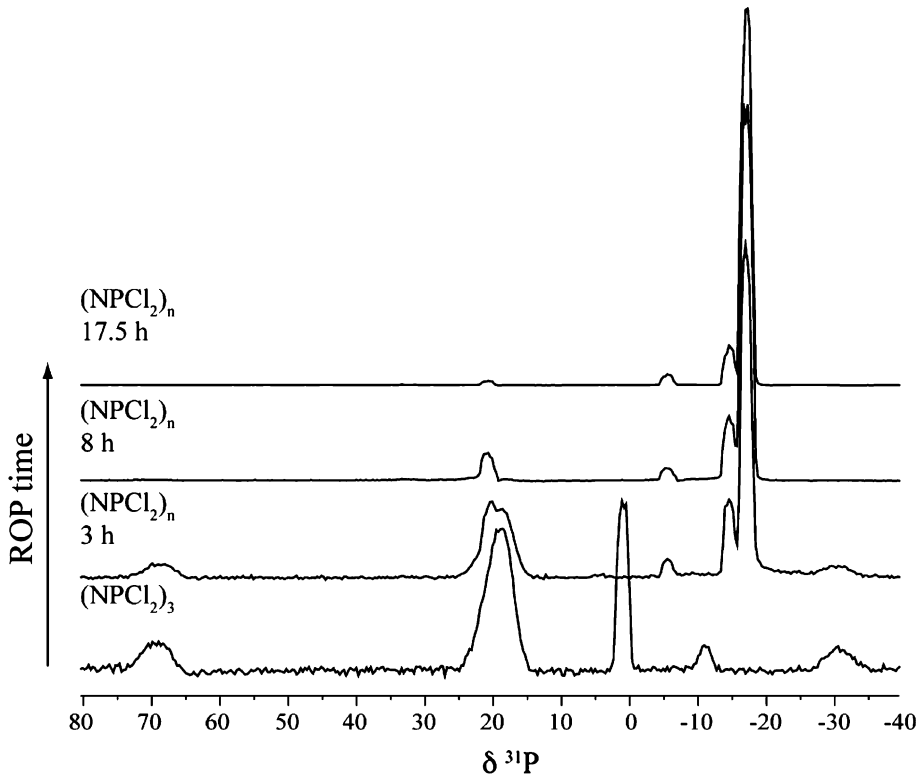

Fig. 40 One-dimensional 202 MHz ^{31}P MAS NMR spectra of the reaction mixture during different stages of the thermal ring-opening polymerization of hexachlorocyclotriphosphazene. (MAS rate = 10 kHz)

sequences have made it possible to adjust experiments to the challenges that inorganic materials present. We believe that advanced solid-state NMR experiments possess tremendous potential for characterizing inorganic polymers and can provide valuable information at the molecular level. Thus, SSNMR spectroscopy can be utilized to enhance the understanding of various properties of inorganic polymers which are difficult to probe by other methods.

Acknowledgements We thank the Natural Sciences and Engineering Research Council (NSERC) of Canada and the University of Lethbridge for financial support. We wish to thank Professor Alec Bain for helpful discussions and suggestions.

References

1. H.W. Spiess, J. Polym. Sci. **42**, 5031–5044 (2004)
2. R.T. Berendt, D.M. Sperger, P.K. Isbester, E.J. Munson, TrAC, Trends Anal. Chem. **25**, 977–984 (2006)
3. E.R. deAzevedo, T.J. Bonagamba, Braz. J. Phys. **36**, 61–74 (2006)
4. C. Odin, in *Annual Reports on NMR Spectroscopy*, vol. 59, 1st edn., ed. by G.A. Webb (Academic Press, London, 2006)
5. S.P. Brown, Macromol. Rapid Commun. **30**, 688–716 (2009)
6. M. Geppi, S. Borsacchi, G. Mollica, C.A. Veracini, Appl. Spectrosc. Rev. **44**, 1–89 (2009)
7. K. Schmidt-Rohr, H.W. Spiess, *Multidimensional Solid-State NMR and Polymers* (Academic Press, San Diego, 1999)
8. K. Aimi, S. Ando, Magn. Reson. Chem. **42**, 577–588 (2004)
9. F.E. Porbeni, I.D. Shin, X.T. Shuai, X.W. Wang, J.L. White, X. Jia, A.E. Tonelli, J. Polym. Sci. B **43**, 2086–2096 (2005)
10. L.Y. Wang, P.F. Fang, C.H. Ye, J.W. Feng, J. Polym. Sci. B **44**, 2864–2879 (2006)
11. A. Asano, Kobunshi Ronbunshu **64**, 406–418 (2007)
12. Q. Chen, K. Schmidt-Rohr, Macromol. Chem. Phys. **208**, 2189–2203 (2007)
13. H. Tatsuno, K. Aimi, S. Ando, Magn. Reson. Chem. **45**, 401–409 (2007)
14. G. Ye, C.A. Hayden, G.R. Goward, Macromolecules **40**, 1529–1537 (2007)
15. L.M. Zhang, H.R. Tang, G.J. Hou, Y.D. Shen, F. Deng, Polymer **48**, 2928–2938 (2007)
16. H. Kurosu, Y. Yamamoto, A. Fujikawa, E. Kawabata, M. Sone, N. Naga, J. Mol. Struct. **921**, 208–214 (2009)
17. A.R. Albunia, R. Graf, A. Grassi, G. Guerra, H.W. Spiess, Macromolecules **42**, 4929–4931 (2009)
18. J. Lu, P.A. Mirau, A.E. Tonelli, Prog. Polym. Sci. **27**, 357–401 (2002)
19. S.S. Jang, V. Molinero, T. Cagin, W.A. Goddard, J. Phys. Chem. B **108**, 3149–3157 (2004)
20. G. Ye, N. Janzen, G.R. Goward, Macromolecules **39**, 3283–3290 (2006)
21. Y.J. Lee, B. Bingol, T. Murakhtina, D. Sebastiani, W.H. Meyer, G. Wegner, H.W. Spiess, J. Phys. Chem. B **111**, 9711–9721 (2007)
22. J.W. Traer, G.R. Goward, Magn. Reson. Chem. **45**, S135–S143 (2007)
23. G. Ye, C.M. Mills, G.R. Goward, J. Membr. Sci. **319**, 238–243 (2008)
24. U. Akbey, R. Graf, Y.G. Peng, P.P. Chu, H.W. Spiess, J. Polym. Sci. B **47**, 138–155 (2009)
25. L. Ghassemadeh, M. Marrony, R. Barrera, K.D. Kreuer, J. Maier, K. Muller, J. Power Sour. **186**, 334–338 (2009)
26. U. Akbey, R. Graf, P.P. Chu, H.W. Spiess, Aust. J. Chem. **62**, 848–856 (2009)
27. G. Brunklaus, S. Schauff, D. Markova, M. Klapper, K. Mullen, H.W. Spiess, J. Phys. Chem. B **113**, 6674–6681 (2009)
28. M. Murakami, H. Ishida, H. Kaji, F. Horii, Polym. J. **36**, 403–412 (2004)
29. M. Murakami, H. Ishida, H. Kaji, F. Horii, M. Tokita, J. Watanabe, Polym. J. **36**, 830–840 (2004)
30. B.R. Cherry, C.H. Fujimoto, C.J. Cornelius, T.M. Alam, Macromolecules **38**, 1201–1206 (2005)
31. X.Q. Zhang, M.D. Do, P. Hoobin, I. Burgar, Polymer **47**, 5888–5896 (2006)
32. A.S. Borisov, P. Hazendonk, P.G. Hayes, J. Inorg. Organomet. Polym. Mater. **18**, 163–174 (2008)
33. P. Hazendonk, C. deDenus, A. Iuga, P. Cahoon, B. Nilsson, D. Iuga, J. Inorg. Organomet. Polym. Mater. **16**, 343–357 (2006)
34. Y.F. Yao, R. Graf, H.W. Spiess, S. Rastogi, Macromolecules **41**, 2514–2519 (2008)
35. K. Saalwachter, I. Schnell, Solid State Nucl. Magn. Reson. **22**, 154–187 (2002)
36. S.F. Liu, J.D. Mao, K. Schmidt-Rohr, J. Magn. Reson. **155**, 15–28 (2002)
37. A. Lesage, PCCP **11**, 6876–6891 (2009)
38. M.H. Levitt, *Spin Dynamics: Basics of Nuclear Magnetic Resonance* (Wiley, Chichester, 2008)
39. E.D. Becker, *High Resolution NMR. Theory and Chemical Applications* (Academic Press, San Diego, 2000)
40. S.E. Ashbrook, PCCP **11**, 6892–6905 (2009)
41. A. Jerschow, Monatsh. Chem. **133**, 1481–1496 (2002)
42. G. Wu, Biochem. Cell Biol. **76**, 429–442 (1998)
43. E.R. Andrew, A. Bradbury, R.G. Eades, Nature **182**, 1659 (1958)
44. E.R. Andrew, A. Bradbury, R.G. Eades, Nature **183**, 1802–1803 (1959)
45. I.J. Lowe, Phys. Rev. Lett. **2**, 285–287 (1959)
46. J. Schaefer, E.O. Stejskal, J. Am. Chem. Soc. **98**, 1031–1032 (1976)
47. A.E. Bennett, C.M. Rienstra, M. Auger, K.V. Lakshmi, R.G. Griffin, J. Chem. Phys. **103**, 6951–6958 (1995)
48. B.C. Gerstein, in *Encyclopedia of Nuclear Magnetic Resonance*, 2nd edn., ed. by D.M. Grant, R.K. Harris (Wiley, Chichester, 2002)
49. A. Lesage, D. Sakellariou, S. Hediger, B. Elena, P. Charmont, S. Steuernagel, L. Emsley, J. Magn. Reson. **163**, 105–113 (2003)
50. S. Paul, R.S. Thakur, M. Goswami, A.C. Sauerwein, S. Mamone, M. Concistre, H. Forster, M.H. Levitt, P.K. Madhu, J. Magn. Reson. **197**, 14–19 (2009)
51. E. Salager, R.S. Stein, S. Steuernagel, A. Lesage, B. Elena, L. Emsley, Chem. Phys. Lett. **469**, 336–341 (2009)
52. A. Bielecki, A.C. Kolbert, M.H. Levitt, Chem. Phys. Lett. **155**, 341–346 (1989)
53. J.P. Amoureux, B. Hu, J. Trebosc, J. Magn. Reson. **193**, 305–307 (2008)
54. M. Leskes, P.K. Madhu, S. Vega, J. Magn. Reson. **199**, 208–213 (2009)
55. E. Vinogradov, P.K. Madhu, S. Vega, Chem. Phys. Lett. **314**, 443–450 (1999)
56. E. Vinogradov, P.K. Madhu, S. Vega, Chem. Phys. Lett. **354**, 193–202 (2002)
57. M. Ernst, J. Magn. Reson. **162**, 1–34 (2003)
58. S.V. Dvinskikh, H. Zimmermann, A. Maliniak, D. Sandstrom, J. Chem. Phys. **122**, (2005)
59. S.F. Liu, K. Schmidt-Rohr, Macromolecules **34**, 8416–8418 (2001)

60. H.E. Bleich, J.A. Glasel, J. Magn. Reson. **35**, 295–299 (1979)
61. T.M. Connor, *NMR Basic Principles and Progress* (Springer-Verlag Telos, Emeryville, 1971)
62. A. Schwenk, in *Encyclopedia of Nuclear Magnetic Resonance*, 2nd edn., ed. by D.M. Grant, R.K. Harris (Wiley, Chichester, 2002)
63. M.J. Duer, *Solid-State NMR. Spectroscopy. Principles and Applications* (Blackwell Science, Oxford, 2002)
64. B. Blumich, D. Ziessow, Mol. Phys. **48**, 955–968 (1983)
65. H. Geen, R. Freeman, J. Magn. Reson. **87**, 415–421 (1990)
66. Y. Manassen, G. Navon, C.T.W. Moonen, J. Magn. Reson. **72**, 551–555 (1987)
67. I. Pelczer, S. Szalma, Chem. Rev. **91**, 1507–1524 (1991)
68. H.W. Spiess, Abstract Paper Am. Chem. Soc. **202**, 137-PHYS (1991).
69. A. Bax, R. Freeman, T.A. Frenkiel, J. Am. Chem. Soc. **103**, 2102–2104 (1981)
70. A. Brinkmann, A.P.M. Kentgens, T. Anupold, A. Samoson, J. Chem. Phys. **129** (2008)
71. G. De Paepe, J.R. Lewandowski, R.G. Griffin, J. Chem. Phys. **128** (2008)
72. J.M. Griffiths, R.G. Griffin, Anal. Chim. Acta **283**, 1081–1101 (1993)
73. J.D. Gross, D.E. Warschawski, R.G. Griffin, J. Am. Chem. Soc. **119**, 796–802 (1997)
74. B. Hu, J. Trebosc, J.P. Amoureux, J. Magn. Reson. **192**, 112–122 (2008)
75. T. Gullion, J. Schaefer, J. Magn. Reson. **81**, 196–200 (1989)
76. B. Arshava, M. Breslav, O. Antohi, R.E. Stark, J.R. Garbow, J.M. Becker, F. Naider, Solid State Nucl. Magn. Reson. **14**, 117–136 (1999)
77. Z.H. Gan, J. Magn. Reson. **183**, 235–241 (2006)
78. F.G. Vogt, S.M. Mattingly, J.M. Gibson, K.T. Mueller, J. Magn. Reson. **147**, 26–35 (2000)
79. M. Feike, D.E. Demco, R. Graf, J. Gottwald, S. Hafner, H.W. Spiess, J. Magn. Reson. A **122**, 214–221 (1996)
80. W. Sommer, J. Gottwald, D.E. Demco, H.W. Spiess, J. Magn. Reson. A **113**, 131–134 (1995)
81. M.J. Bayro, R. Ramachandran, M.A. Caporini, M.T. Eddy, R.G. Griffin, J. Chem. Phys. **128** (2008)
82. A.E. Bennett, C.M. Rienstra, J.M. Griffiths, W.G. Zhen, P.T. Lansbury, R.G. Griffin, J. Chem. Phys. **108**, 9463–9479 (1998)
83. C.P. Grey, W.S. Veeman, A.J. Vega, J. Chem. Phys. **98**, 7711–7724 (1993)
84. C.P. Grey, A.J. Vega, J. Am. Chem. Soc. **117**, 8232–8242 (1995)
85. E.R.H. Vaneck, R. Janssen, W. Maas, W.S. Veeman, Chem. Phys. Lett. **174**, 428–432 (1990)
86. Y. Ba, H.M. Kao, G.P. Grey, L. Chopin, T. Gullion, J. Magn. Reson. **133**, 104–114 (1998)
87. G.P. Holland, T.M. Alam, PCCP **7**, 1739–1742 (2005)
88. W.L. Huang, A.J. Vega, T. Gullion, T. Polenova, J. Am. Chem. Soc. **129**, 13027–13034 (2007)
89. E. Hughes, T. Gullion, A. Goldbourt, S. Vega, A.J. Vega, J. Magn. Reson. **156**, 230–241 (2002)
90. R. Tycko, G. Dabbagh, Chem. Phys. Lett. **173**, 461–465 (1990)
91. A.W. Hing, S. Vega, J. Schaefer, J. Magn. Reson. **96**, 205–209 (1992)
92. A.W. Hing, S. Vega, J. Schaefer, J. Magn. Reson. A **103**, 151–162 (1993)
93. A. Brinkmann, M. Eden, M.H. Levitt, J. Chem. Phys. **112**, 8539–8554 (2000)
94. A. Brinkmann, M.H. Levitt, J. Chem. Phys. **115**, 357–384 (2001)
95. P.E. Kristiansen, M. Carravetta, W.C. Lai, M.H. Levitt, Chem. Phys. Lett. **390**, 1–7 (2004)
96. P.E. Kristiansen, M. Carravetta, J.D. van Beek, W.C. Lai, M.H. Levitt, J. Chem. Phys. **124**, 1–19 (2006)
97. P.K. Madhu, X. Zhao, M.H. Levitt, Chem. Phys. Lett. **346**, 142–148 (2001)
98. I. Marin-Montesinos, D.H. Brouwer, G. Antonioli, W.C. Lai, A. Brinkmann, M.H. Levitt, J. Magn. Reson. **177**, 307–317 (2005)
99. J.D. van Beek, R. Dupree, M.H. Levitt, J. Magn. Reson. **179**, 38–48 (2006)
100. X. Zhao, M. Eden, M.H. Levitt, Chem. Phys. Lett. **342**, 353–361 (2001)
101. X. Zhao, W. Hoffbauer, J. Gunne, M.H. Levitt, Solid State Nucl. Magn. Reson. **26**, 57–64 (2004)
102. J. Battiste, R.A. Newmark, Prog. Nucl. Magn. Reson. Spectrosc. **48**, 1–23 (2006)
103. R.A. Newmark, J.L. Battiste, M.I. Koivula, Abstract Paper Am. Chem. Soc. **221**, 286-POLY (2001).
104. A. Ramamoorthy, C.H. Wu, S.J. Opella, J. Magn. Reson. **140**, 131–140 (1999)
105. J. Rocha, C.M. Morais, C. Fernandez, in *New Techniques in Solid-State NMR*, 1st edn., ed. by J. Klinowski (Springer, Berlin, 2005)
106. F. Fayon, I.J. King, R.K. Harris, J.S.O. Evans, D. Massiot, C.R. Chim. **7**, 351–361 (2004)
107. L.A. O'Dell, E.A. Abou Neel, J.C. Knowles, M.E. Smith, Mater. Chem. Phys. **114**, 1008–1015 (2009)
108. L.A. O'Dell, P. Guerry, A. Wong, E.A. Abou Neel, T.N. Pham, J.C. Knowles, S.P. Brown, M.E. Smith, Chem. Phys. Lett. **455**, 178–183 (2008)
109. A.B. Bose, M. Gangoda, M. Jaroniec, R.K. Gilpin, R.N. Bose, Surf. Sci. **600**, 143–154 (2006)
110. A.S. Brar, K. Dutta, Polym. J. **30**, 304–310 (1998)
111. M.H. Chisholm, S.S. Iyer, D.G. McCollum, M. Pagel, U. Werner-Zwanziger, Macromolecules **32**, 963–973 (1999)
112. S.S. Hou, T.J. Bonagamba, F.L. Beyer, P.H. Madison, K. Schmidt-Rohr, Macromolecules **36**, 2769–2776 (2003)
113. X. Jia, X.W. Wang, A.E. Tonelli, J.L. White, Macromolecules **38**, 2775–2780 (2005)
114. J.E. Kasperczyk, Polymer **40**, 5455–5458 (1999)
115. R. Kiebooms, P. Adriaensens, D. Vanderzande, J. Gelan, M.J. Swann, D. Bloor, C.J. Drury, G.M. Brooke, Macromolecules **29**, 5981–5989 (1996)
116. S. Li, D.M. Rice, F.E. Karasz, Macromolecules **27**, 2211–2218 (1994)
117. A.V. Lubnin, J.P. Kennedy, J. Macromol. Sci. Pure Appl. Chem. **A32**, 191–210 (1995)
118. R. Luliucci, C. Taylor, W.K. Hollis, Magn. Reson. Chem. **44**, 375–384 (2006)
119. K. Murata, H. Kono, E. Katoh, S. Kuroki, I. Ando, Polymer **44**, 4021–4027 (2003)
120. A. Sroka-Bartnicka, S. Olejniczak, W. Ciesielski, A. Nosal, H. Szymanowski, M. Gazicki-Lipman, M.J. Potrzebowski, J. Phys. Chem. **B113**, 5464–5472 (2009)
121. M. Suchoparek, J. Spevacek, B. Masar, Polymer **35**, 3389–3397 (1994)
122. J.L. White, A.J. Dias, J.R. Ashbaugh, Macromolecules **31**, 1880–1888 (1998)
123. M.T. Zell, B.E. Padden, A.J. Paterick, K.A.M. Thakur, R.T. Kean, M.A. Hillmyer, E.J. Munson, Macromolecules **35**, 7700–7707 (2002)
124. X.D. Zhao, L. Zhu, J.B. Huang, X.J. Xu, Y. Pan, J. Fluorine Chem. **126**, 883–887 (2005)
125. S.P. Brown, A. Lesage, B. Elena, L. Emsley, J. Am. Chem. Soc. **126**, 13230–13231 (2004)
126. C. Coelho, T. Azais, L. Bonhomme-Coury, G. Laurent, C. Bonhomme, Inorg. Chem. **46**, 1379–1387 (2007)

127. B. Elena, A. Lesage, S. Steuernagel, A. Bockmann, L. Emsley, J. Am. Chem. Soc. **127**, 17296–17302 (2005)
128. A. Bax, M.F. Summers, J. Am. Chem. Soc. **108**, 2093–2094 (1986)
129. A. Lesage, L. Emsley, J. Magn. Reson. **148**, 449–454 (2001)
130. A. Lesage, D. Sakellariou, S. Steuernagel, L. Emsley, J. Am. Chem. Soc. **120**, 13194–13201 (1998)
131. K. Schmidtrohr, Abstract Paper Am. Chem. Soc. 208, 111-PMSE (1994).
132. W.G. Hiller, H. Schneider, V.D. Fedotov, J. Polym. Sci. B **30**, 931–942 (1992)
133. S. Kitazawa, T. Hiraoki, T. Hamada, A. Tsutsumi, Polym. J. **26**, 1213–1226 (1994)
134. T.R. Lutz, Y.Y. He, M.D. Ediger, Macromolecules **38**, 9826–9835 (2005)
135. K.L. Ngai, C.M. Roland, Macromolecules **37**, 2817–2822 (2004)
136. X.H. Qiu, M.D. Ediger, J. Polym. Sci. B **38**, 2634–2643 (2000)
137. V.V. Rodin, A.V. Kharenko, B.V. Sakharov, V.A. Kemenova, O.N. Abroskina, A.A. Kurakina, Colloid J. **56**, 61–65 (1994)
138. I.D. Shin, L. Huang, A.E. Tonelli, Macromol. Symp. **138**, 21–40 (1999)
139. S. Yoshioka, Y. Aso, T. Otsuka, S. Kojima, J. Pharm. Sci. **84**, 1072–1077 (1995)
140. M. Gentzler, S. Patil, J.A. Reimer, M.M. Denn, Solid State Nucl. Magn. Reson. **12**, 97–112 (1998)
141. A. Naito, A. Fukutani, M. Uitdehaag, S. Tuzi, H. Saito, J. Mol. Struct. **441**, 231–241 (1998)
142. G.H. Penner, B.Y. Zhao, K.R. Jeffrey, Z. Naturforsch A **50**, 81–89 (1995)
143. D.L. Tzou, P. Desai, A.S. Abhiraman, T.H. Huang, J. Polym. Sci. B **29**, 49–56 (1991)
144. S. Ando, R.K. Harris, G.A. Monti, S.A. Reinsberg, Magn. Reson. Chem. **37**, 709–720 (1999)
145. S. Ando, R.K. Harris, S.A. Reinsberg, J. Magn. Reson. **141**, 91–103 (1999)
146. D.E. Favre, D.J. Schaefer, B.F. Chmelka, J. Magn. Reson. **134**, 261–279 (1998)
147. D. Huster, L. Naji, J. Schiller, K. Arnold, Appl. Magn. Reson. **27**, 471–487 (2004)
148. H. Kaji, K. Fuke, F. Horii, Macromolecules **36**, 4414–4423 (2003)
149. H. Kaji, T. Tai, F. Horii, Macromolecules **34**, 6318–6324 (2001)
150. T. Miyoshi, S. Hayashi, F. Imashiro, A. Kaito, Macromolecules **35**, 2624–2632 (2002)
151. K. Schmidtrohr, in *Multidimensional Spectroscopy of Polymers—Vibrational, NMR, and Fluorescence Techniques*, ed. by M.W. Urban, T. Provder (American Chemical Society, Washington, DC, 1995)
152. M. Gaborieau, R. Graf, S. Kahle, T. Pakula, H.W. Spiess, Macromolecules **40**, 6249–6256 (2007)
153. W. Gabrielse, H.A. Gaur, F.C. Feyen, W.S. Veeman, Macromolecules **27**, 5811–5820 (1994)
154. S. Gandhi, C. Melian, D.E. Demco, A.S. Brar, B. Blumich, Macromol. Chem. Phys. **209**, 1576–1585 (2008)
155. N. Le Bouch, M. Auger, M. Leclerc, Macromol. Chem. Phys. **209**, 2455–2462 (2008)
156. K. Saalwachter, Prog. Nucl. Magn. Reson. Spectrosc. **51**, 1–35 (2007)
157. H. Tatsuno, Y. Koseki, S. Ando, Polymer **49**, 2709–2716 (2008)
158. M.T. Wang, G.M. Bernard, R.E. Wasylishen, P. Choi, Macromolecules **40**, 6594–6599 (2007)
159. J.R. Wickham, R.N. Mason, C.V. Rice, Solid State Nucl. Magn. Reson. **31**, 184–192 (2007)
160. Y. F. Yao, R. Graf, H. W. Spiess, D. R. Lippits and S. Rastogi, Phys. Rev. E: Stat. Phys. Plasmas Fluids Relat. Interdisciplin. Top. **76** (2007).
161. B. Zhu, W.H. Kai, P.J. Pan, K. Yazawa, H. Nishida, M. Sakurai, Y. Inoue, J. Phys. Chem. B **112**, 9684–9692 (2008)
162. D. Reichert, G. Hempel, H. Zimmermann, H. Schneider, Z. Luz, Solid State Nucl. Magn. Reson. **18**, 17–36 (2000)
163. K. Saalwachter, J.U. Sommer, Macromol. Rapid Commun. **28**, 1455–1465 (2007)
164. N.A. Vaz, M.J. Vaz, J.W. Doane, Phys. Rev. A **30**, 1008–1016 (1984)
165. K. Schmidt-Rohr, E.R. deAzevedo, T.J. Bonagamba, in *Encyclopedia of Nuclear Magnetic Resonance*, 2nd edn., ed. by D.M. Grant, R.K. Harris (Wiley, Chichester, 2002)
166. S. Ando, R.K. Harris, P. Hazendonk, P. Wormald, Macromol. Rapid Commun. **26**, 345–356 (2005)
167. M. Bertmer, D.E. Demco, M. Wang, C. Melian, R.I. Marcean-Chelcea, R. Fechete, M. Baias, B. Blumich, Chem. Phys. Lett. **431**, 404–409 (2006)
168. J. Clauss, K. Schmidtrohr, H. W. Spiess, Acta Polym. **44**, 1–17 (1993)
169. F.M. Mulder, W. Heinen, M. van Duin, J. Lugtenburg, H.J.M. de Groot, J. Am. Chem. Soc. **120**, 12891–12894 (1998)
170. D.J. Harris, E.R. de Azevedo, T.J. Bonagamba, J. Magn. Reson. **162**, 67–73 (2003)
171. F.A. Bovey, P.A. Mirau, *NMR of Polymers* (Academic Press, San-Diego, 1996)
172. P. Caravatti, P. Neuenschwander, R.R. Ernst, Macromolecules **19**, 1889–1895 (1986)
173. N. Egger, K. Schmidtrohr, B. Blumich, W.D. Domke, B. Stapp, J. Appl. Polym. Sci. **44**, 289–295 (1992)
174. A.E. Bennett, C.M. Rienstra, P.T. Lansbury, R.G. Griffin, J. Chem. Phys. **105**, 10289–10299 (1996)
175. J. Gunne, J. Magn. Reson. **180**, 186–196 (2006)
176. J.D. Mao, K. Schmidt-Rohr, J. Magn. Reson. **162**, 217–227 (2003)
177. K.T. Mueller, J. Magn. Reson. A **113**, 81–93 (1995)
178. W. Maas, W.A.C. Vanderheijden, W.S. Veeman, J.M.J. Vankan, G.H.W. Buning, J. Chem. Phys. **95**, 4698–4708 (1991)
179. W.E. Maas, in *Multidimensional Spectroscopy of Polymers—Vibrational, NMR, and Fluorescence Techniques*, 1st edn., ed. by M.W. Urban, T. Provder (American Chemical Society, Washington, DC, 1995)
180. R. Sangill, N. Rastrupandersen, H. Bildsoe, H.J. Jakobsen, N.C. Nielsen, J. Magn. Reson. A **107**, 67–78 (1994)
181. S. Ando, R.K. Harris, P. Holstein, S.A. Reinsberg, K. Yamauchi, Polymer **42**, 8137–8151 (2001)
182. S. Ando, R.K. Harris, S.A. Reinsberg, Magn. Reson. Chem. **40**, 97–106 (2002)
183. P. Hazendonk, R.K. Harris, S. Ando, P. Avalle, J. Magn. Reson. **162**, 206–216 (2003)
184. P. Hazendonk, P. Wormald, T. Montina, J. Phys. Chem. A **A112**, 6262–6274 (2008)
185. P. Wormald, B. Ameduri, R.K. Harris, P. Hazendonk, Solid State Nucl. Magn. Reson. **30**, 114–123 (2006)
186. P. Caravatti, P. Neuenschwander, R.R. Ernst, Macromolecules **18**, 119–122 (1985)
187. R.A. Assink, Macromolecules **11**, 1233–1237 (1978)
188. A. Buda, D.E. Demco, M. Bertmer, B. Blumich, V.M. Litvinov, J.P. Penning, J. Phys. Chem. B **B107**, 5357–5370 (2003)
189. A. Buda, D.E. Demco, M. Bertmer, B. Blumich, B. Reining, H. Keul, H. Hocker, Solid State Nucl. Magn. Reson. **24**, 39–67 (2003)
190. Q. Chen, K. Schmidt-Rohr, Solid State Nucl. Magn. Reson. **29**, 142–152 (2006)
191. T.T.P. Cheung, B.C. Gerstein, J. Appl. Phys. **52**, 5517–5528 (1981)
192. D.E. Demco, A. Johansson, J. Tegenfeldt, Solid State Nucl. Magn. Reson. **4**, 13–38 (1995)

193. R.R. Eckman, P.M. Henrichs, A.J. Peacock, Macromolecules **30**, 2474–2481 (1997)
194. G. Meresi, Y. Wang, A. Bandis, P.T. Inglefield, A.A. Jones, W.Y. Wen, Polymer **42**, 6153–6160 (2001)
195. S.A. Taylor, J.L. White, N.C. Elbaum, R.C. Crosby, G.C. Campbell, J.F. Haw, G.R. Hatfield, Macromolecules **25**, 3369–3376 (1992)
196. D.L. VanderHart, Y. Feng, C.C. Han, R.A. Weiss, Macromolecules **33**, 2206–2227 (2000)
197. M. Goldman and L. Shen, Phys. Rev. 144, 321-& (1966).
198. J. Clauss, K. Schmidtrohr, A. Adam, C. Boeffel, H.W. Spiess, Macromolecules **25**, 5208–5214 (1992)
199. K. Schmidtrohr, J. Clauss, B. Blumich, H.W. Spiess, Magn. Reson. Chem. **28**, S3–S9 (1990)
200. K. Schmidtrohr, J. Clauss, B. Blumich, H.W. Spiess, Abstract Paper Am. Chem. Soc. 199, 284-POLY (1990).
201. K. Schmidtrohr, J. Clauss, H.W. Spiess, Macromolecules **25**, 3273–3277 (1992)
202. A.E. Aliev, R.V. Law, Nucl. Magn. Reson. **38**, 271–321 (2009)
203. M.W. Pitcher, Y. Arslan, P. Edinc, M. Hartal, M. Masjedi, O. Metin, F. Sen, O. Turkarslan, B. Yigitsoy, Phosphorus Sulfur Silicon Relat. Elem. **182**, 2861–2880 (2007)
204. A. Rahimi, Iran Polym. J. **13**, 149–164 (2004)
205. J. Chojnowski, M. Cypryk, J. Kurjata, Prog. Polym. Sci. **28**, 691–728 (2003)
206. J.E. Mark, H.R. Allcock, R. West, *Inorganic Polymers* (Oxford University Press, New York, 2004)
207. A. Mustafa, M. Achilleos, J. Ruiz-Iban, J. Davies, R.E. Benfield, R.G. Jones, D. Grandjean, S.J. Holder, React. Funct. Polym. **66**, 123–135 (2006)
208. L. Sacarescu, R. Ardeleanu, G. Sacarescu, M. Simionescu, High Perform. Polym. **19**, 510–519 (2007)
209. L. Sacarescu, R. Ardeleanu, G. Sacarescu, M. Simionescu, I. Mangalagiu, High Perform. Polym. **19**, 501–509 (2007)
210. J.G. Zhou, A. Addison, Z. He, F. Wang, Mater. Des. **26**, 670–679 (2005)
211. G.N. Babu, R.A. Newmark, Macromolecules **24**, 4503–4509 (1991)
212. R. Dabek, J. Cervantes, A. Zizumbo, Macromol. Symp. **148**, 121–129 (1999)
213. M. Elangovan, A. Muthukumaran, M.A. Kulandainathan, Eur. Polym. J. **41**, 2450–2460 (2005)
214. E. Fossum, K. Matyjaszewski, Macromolecules **28**, 1618–1625 (1995)
215. B.J. Grimmond, J.Y. Corey, Organometallics **18**, 2223–2229 (1999)
216. D.J. Liaw, D.L. Ou, J. Appl. Polym. Sci. **62**, 9–14 (1996)
217. X. Mao, Y. Song, Acta Polym. 1141–1148 (2007)
218. K. Matyjaszewski, J. Chrusciel, J. Maxka, M. Sasaki, J. Inorg. Organomet. Polym. **5**, 261–279 (1995)
219. Q.F. Si, X. Wang, X.D. Fan, S.J. Wang, J. Polym. Sci. A **43**, 1883–1894 (2005)
220. W. Uhlig, J. Polym. Sci. A **33**, 239–246 (1995)
221. Z.F. Zhang, F. Babonneau, R.M. Laine, Y. Mu, J.F. Harrod, J.A. Rahn, J. Am. Ceram. Soc. **74**, 670–673 (1991)
222. M. Cypry, Polimery **52**, 730–735 (2007)
223. R.K. Harris, K. Metcalfe, E. Hengge, Polyhedron **4**, 1319–1321 (1985)
224. T. Takayama, I. Ando, J. Mol. Struct. **222**, 275–283 (1990)
225. T. Takayama, S. Ando, I. Ando, J. Mol. Struct. **220**, 243–250 (1990)
226. A.J. Lovinger, D.D. Davis, F.C. Schilling, F.J. Padden, F.A. Bovey, J.M. Zeigler, Macromolecules **24**, 132–139 (1991)
227. R. Menescal, J. Eveland, R. West, L.L. Leites, S.S. Bukalov, T.D. Yadritseva, M. Blazso, Macromolecules **27**, 5885–5892 (1994)
228. F. Babonneau, R. Richter, C. Bonhomme, J. Maquet, G. Roewer, J. Chim, Phys. Phys. Chim. Biol. **92**, 1745–1748 (1995)
229. F. Babonneau, J. Maquet, C. Bonhomme, R. Richter, G. Roewer, D. Bahloul, Chem. Mater. **8**, 1415–1428 (1996)
230. T. Takayama, J. Mol. Struct. **441**, 101–117 (1998)
231. R.D. O'Connor, F.D. Blum, E. Ginsburg, R.D. Miller, Macromolecules **31**, 4852–4861 (1998)
232. C. Mueller, H. Frey, C. Schmidt, Monatsh. Chem. **130**, 175–180 (1999)
233. R. Bischoff, S.E. Cray, Prog. Polym. Sci. **24**, 185–219 (1999)
234. A. Rahimi, P. Shokrolahi, Int. J. Inorg. Mater. **3**, 843–847 (2001)
235. Y. Abe, T. Gunji, Prog. Polym. Sci. **29**, 149–182 (2004)
236. J. Chrusciel, E. Lesniak, M. Fejdys, Polimery **53**, 817–829 (2008)
237. W.Z. Cai, K. Schmidtrohr, N. Egger, B. Gerharz, H.W. Spiess, Polymer **34**, 267–276 (1993)
238. J. Brus, J. Dybal, Polymer **41**, 5269–5282 (2000)
239. J. Brus, J. Sol-Gel Sci. Technol. **25**, 17–28 (2002)
240. J. Brus, J. Dybal, Macromolecules **35**, 10038–10047 (2002)
241. W.J. Liang, C.L. Kuo, C.L. Lin, P.L. Kuo, J. Polym. Sci. A **40**, 1226–1235 (2002)
242. D. Seyferth, G.H. Wiseman, J.M. Schwark, Y.-F. Yu, C.A. Poutasse, in *Inorganic and Organometallic Polymers. Macromolecules Containing Silicon, Phosphorous, and Other Inorganic Elements*, 1st edn., ed. by M. Zeldin, K.J. Wynne, H.R. Allcock (American Chemical Society, Washington, DC, 1988)
243. J.L. He, M. Scarlete, J.F. Harrod, J. Am. Ceram. Soc. **78**, 3009–3017 (1995)
244. J. Seitz, J. Bill, N. Egger, F. Aldinger, J. Eur. Ceram. Soc. **16**, 885–891 (1996)
245. D. Bahloul, M. Pereira, C. Gerardin, J. Mater. Chem. **7**, 109–116 (1997)
246. M.R. Mucalo, N.B. Milestone, I.W.M. Brown, J. Mater. Sci. **32**, 2433–2444 (1997)
247. Y.L. Li, E. Kroke, R. Riedel, C. Fasel, C. Gervais, F. Babonneau, Appl. Organomet. Chem. **15**, 820–832 (2001)
248. S. Trassl, H.J. Kleebe, H. Stormer, G. Motz, E. Rossler, G. Ziegler, J. Am. Ceram. Soc. **85**, 1268–1274 (2002)
249. M. Horz, A. Zern, F. Berger, J. Haug, K. Muller, F. Aldinger, M. Weinmann, J. Eur. Ceram. Soc. **25**, 99–110 (2005)
250. E. Brendler, E. Ebrecht, B. Thomas, G. Boden, T. Breuning, Fresenius J. Anal. Chem. **363**, 185–188 (1999)
251. W.R. Schmidt, D.M. Narsavage-Heald, D.M. Jones, P.S. Marchetti, D. Raker, G.E. Maciel, Chem. Mater. **11**, 1455–1464 (1999)
252. F. Berger, M. Weinmann, F. Aldinger, K. Muller, Chem. Mater. **16**, 919–929 (2004)
253. J. Schuhmacher, F. Berger, M. Weinmann, J. Bill, F. Aldinger, K. Muller, Appl. Organomet. Chem. **15**, 809–819 (2001)
254. N. Janakiraman, M. Weinmann, J. Schuhmacher, K. Muller, J. Bill, F. Aldinger, P. Singh, J. Am. Ceram. Soc. **85**, 1807–1814 (2002)
255. A.S. Abd-El-Aziz, Macromol. Rapid Commun. **23**, 995–1031 (2002)
256. A.S. Abd-El-Aziz, C.E. Carraher, C.U. Pittman, J.E. Sheats, M. Zeldin, Abstract Paper Am. Chem. Soc. 223, 207-PMSE (2002).
257. A.S. Abd-El-Aziz, E.K. Todd, Coord. Chem. Rev. **246**, 3–52 (2003)
258. A.S. Abd-El-Aziz, C.E. Carraher, C.U. Pittman, M. Zeldin, J.E. Sheats, Abstract Paper Am. Chem. Soc. 230, 455-PMSE (2005).
259. D. Foucher, R. Ziembinski, R. Petersen, J. Pudelski, M. Edwards, Y.Z. Ni, J. Massey, C.R. Jaeger, G.J. Vancso, I. Manners, Macromolecules **27**, 3992–3999 (1994)
260. I. Manners, Chem. Commun. **85**, 7–865 (1999)
261. K.N. Power-Billard, I. Manners, Macromolecules **33**, 26–31 (2000)

262. K. Kulbaba, P.M. Macdonald, I. Manners, Macromolecules **32**, 1321–1324 (1999)
263. K. Kulbaba, P.M. Macdonald, I. Manners, Abstract Paper Am. Chem. Soc. 219, 113-PMSE (2000).
264. K. Kulbaba, I. Manners, P.M. Macdonald, Macromolecules **35**, 10014–10025 (2002)
265. C.M. Widdifield, R.W. Schurko, J. Phys. Chem. A **109**, 6865–6876 (2005)
266. H.R. Allcock, J. Inorg. Organomet. Polym. Mater. **16**, 277–294 (2006)
267. C.H. Honeyman, I. Manners, C.T. Morrissey, H.R. Allcock, J. Am. Chem. Soc. **117**, 7035–7036 (1995)
268. H. R. Allcock and R. L. Kugel, J. Am. Chem. Soc. 87, 4216-& (1965).
269. H. R. Allcock, R. L. Kugel and K. J. Valan, Inorg. Chem. 5, 1709-& (1966).
270. G. Dhalluin, R. Dejaeger, P. Potin, Bull. Soc. Chim. Belg. **98**, 653–665 (1989)
271. G. Dhalluin, R. Dejaeger, J.P. Chambrette, P. Potin, Macromolecules **25**, 1254–1258 (1992)
272. R.G. Pratt, J.L. Ackerman, Abstract Paper Am. Chem. Soc. 186, 61-PMSE (1983).
273. H. Tanaka, M.A. Gomez, A.E. Tonelli, S.V. Chichesterhicks, R.C. Haddon, Macromolecules **21**, 2301–2304 (1988)
274. S.G. Young, J.H. Magill, Macromolecules **22**, 2549–2551 (1989)
275. K. Takegoshi, I. Tanaka, K. Hikichi, S. Higashida, Macromolecules **25**, 3392–3398 (1992)
276. R. Simonutti, A. Comotti, P. Sozzani, J. Inorg. Organomet. Polym. **6**, 313–324 (1996)
277. R. Simonutti, W.S. Veeman, F.C. Ruhnau, M.C. Gallazzi, P. Sozzani, Macromolecules **29**, 4958–4962 (1996)
278. F.F. Stewart, E.S. Peterson, S.C. Busse, C.J. Orme, Chem. Mater. **9**, 155–163 (1997)
279. B. Koch, M. Vogel, Macromolecules **42**, 531–536 (2009)
280. A.S. Borisov, P. Hazendonk, P.G. Hayes, J. Inorg. Organomet. Polym. Mater. ASAP (2009). doi: 10.1007/s10904-009-9316-2

Author Biographies

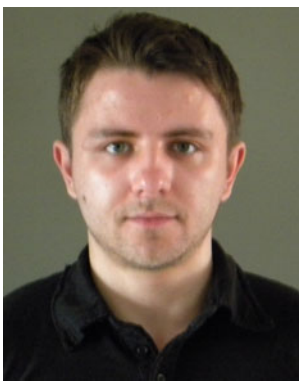

Alexey S. Borisov graduated from the State Technological University, St-Petersburg, Russia with a B.Tech. degree in 2005. He commenced his graduate studies at the University of Lethbridge under the supervision of Dr. Paul Hazendonk and Dr. Paul G. Hayes completing his M.Sc. in 2009 and is currently pursuing his Ph.D in the same group. His research is focused on the synthesis of phosphazene polymers and their characterization by solid-state nuclear magnetic resonance spectroscopy.

Paul Hazendonk obtained his M.Sc. (1995) with Ted P. Schaefer at the University of Manitoba, Winnipeg, Canada, continued his Ph.D. (2000) with Alec D. Bain at McMaster University, Hamilton, Canada, and subsequently completed a post-doctoral fellowship with Robin K. Harris at the University of Durham, Durham, UK. Currently he is an associate professor of chemistry at the University of Lethbridge. An expert in NMR spectroscopy Paul specializes in solid-state NMR developing experimental techniques particularly suited to inorganic materials and fluorine containing systems.

Paul G. Hayes completed his Ph.D. under the tutelage of Prof. Warren Piers at the University of Calgary. In 2004 he undertook an NSERC Postdoctoral Fellowship in the laboratories of Prof. T. Don Tilley. Paul is currently an Associate Professor and Alberta Ingenuity New Faculty at the University of Lethbridge; his current research interests include synthetic and mechanistic organometallic chemistry with a particular focus on the development of new chemical transformations and catalysis.